J. Fluid Mech. (2024), *vol*. 982, A24, doi:10.1017/jfm.2024.117

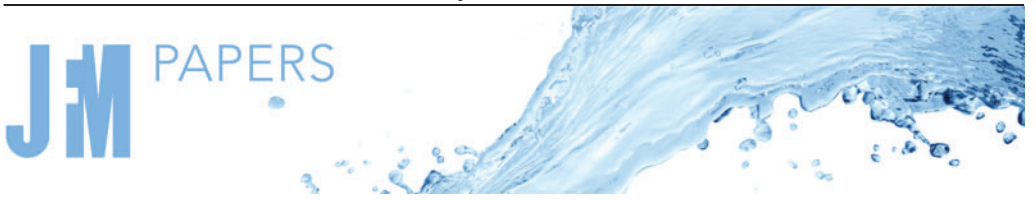

Effect of bulk viscosity on the hypersonic compressible turbulent boundary layer

Chaoyu Zheng[1], **Yongliang Feng**[1,2,†] **and Xiaojing Zheng**[3]

[1]School of Aeronautics, Northwestern Polytechnical University, Xi'an 710072, PR China

[2]Institute of Extreme Mechanics, School of Aeronautics, Northwestern Polytechnical University, Xi'an 710072, PR China

[3]Research Center for Applied Mechanics, Xidian University, Xi'an 710071, PR China

(Received 7 August 2023; revised 28 December 2023; accepted 27 January 2024)

The impact of bulk viscosity is unclear with considering the increased dilatational dissipation and compressibility effects in hypersonic turbulence flows. In this study, we employ direct numerical simulations to conduct comprehensive analysis of the effect of bulk viscosity on hypersonic turbulent boundary layer flow over a flat plate. The results demonstrate that the scaling relations remain valid even when accounting for large bulk viscosity. However, the wall-normal velocity fluctuations v''_{rms} decrease significantly in the viscous sublayer due to the enhanced bulk dilatational dissipation. The intensity of travelling-wave-like alternating positive and negative structures of instantaneous pressure fluctuations p'_{rms} in the near-wall region decreases distinctly after considering the bulk viscosity, which is attributed mainly to the reduction of compressible pressure fluctuations $p^{+}_{c,rms}$. Furthermore, the velocity divergence $\partial u_i/\partial x_i$ undergoes a significant decrease by bulk viscosity. In short, our results indicate that bulk viscosity can weaken the compressibility of the hypersonic turbulent boundary layer and becomes more significant as the Mach number increases and the wall temperature decreases. Notably, when the bulk-to-shear viscosity ratio of the gas reaches a few hundred levels ($\mu_b/\mu = O(10^2)$), and mechanical behaviour of the near-wall region ($y^+ \leq 30$) is of greater interest, the impact of bulk viscosity on the hypersonic cold-wall turbulent boundary layer may not be negligible.

Key words: hypersonic flow, turbulent boundary layers, boundary layer structure

† Email address for correspondence: yongliang.feng@nwpu.edu.cn

1. Introduction

Enhanced knowledge of hypersonic turbulent boundary layers holds significant implications for various aspects of hypersonic vehicle design and performance. In contrast to subsonic/supersonic flight, the higher speed of hypersonic flight results in a significant conversion of kinetic energy into internal energy within the boundary layer. Consequently, it places a greater demand on thermal protection technology for the surfaces of vehicles. In subsonic/supersonic flight, the surface of the vehicle is approximately an adiabatic wall, while the wall temperature of the hypersonic vehicle is significantly lower than that of the adiabatic wall (Duan, Beekman & Martín 2010; Xu *et al.* 2021*b*; Ou, Wang & Chen 2024). The accurate modelling of the wall-cooling and compressibility effects in a hypersonic turbulent boundary layer is of great significance for the prediction of the surface heat flux and the design of the thermal protection of the vehicle (Huang, Duan & Choudhari 2022).

Direct numerical simulations (DNS) play a pivotal role in advancing the understanding of hypersonic boundary layers, which are crucial in the development of hypersonic technology. The DNS allow for highly accurate and detailed simulations, providing a wealth of three-dimensional flow field data. This enables researchers to investigate the complex flow phenomena comprehensively, including small-scale structures near the wall, which are otherwise challenging to access through experimental means. The high Mach numbers and low wall temperatures inherent in hypersonic boundary layers pose unique challenges, and DNS emerge as a powerful tool to tackle these complexities. By conducting DNS studies under various Mach numbers, Reynolds numbers and wall temperature conditions, researchers can gain profound insights into flow physics, turbulence characteristics and heat transfer mechanisms, as evidenced by the studies listed in table 1.

Duan, Beekman & Martín (2011) investigated the effect of the Mach number ($0.3 \leq Ma \leq 12$) on the compressible turbulent flat plate boundary layer, and found that the compressibility of the fluid is enhanced with the increase of Mach number, while the scaling relations remain valid, such as Morkovin's scaling and the strong Reynolds analogy. Subsequently, Lagha *et al.* (2011) further performed DNS of the compressible turbulent boundary layer with Mach number up to 20, and found that the velocity dilatation varies significantly with increasing Mach number, but can still be normalized by considering the average density variation. Duan *et al.* (2010) studied the effect of wall temperature ($0.18 \leq T_w/T_r \leq 1.00$) on the compressible turbulent flat plate boundary layer, and found that the compressibility of the fluid is enhanced by decreasing the wall temperature, while the scaling relations are still suitable. Zhang, Duan & Choudhari (2018) further conducted DNS of compressible turbulent boundary layers with Mach numbers from 2.5 to 14 and wall-to-recovery temperature ratios from 0.18 to 1.0. They evaluated the applicability of the compressibility transformations, and verified the validity of several new scaling laws considering wall heat flux. The results of compressible turbulent boundary layer with Mach numbers from 11 to 14 and wall-to-recovery temperature ratio 0.2 by Huang *et al.* (2020) showed that the algebraic energy flux model can predict the streamwise turbulent heat flux better than the commonly constant turbulent Prandtl number model, based on the good prediction of statistics such as wall-normal turbulent heat flux. For the effect of wall cooling on pressure fluctuations, Zhang *et al.* (2022) found that the cold-wall effect suppressed fast and slow pressures, resulting in a decrease in pressure fluctuations in the subsonic/supersonic case, while enhancing the compressible pressure, especially in the hypersonic case, caused an increase in pressure fluctuations. Cogo *et al.* (2022) studied the effect of high Reynolds number and wall cooling on the supersonic and hypersonic zero pressure gradient turbulent boundary layer, and found

Case	Ma_∞	Re_τ	T_w/T_r	Non-equilibrium effects
Martin (2007)	3–6	—	1.0	
Duan *et al.* (2010)	5	385.9–798.1	0.18–1.00	
Duan *et al.* (2011)	0.3–12	376.3–569.9	1.00	
Duan & Martín (2011)	3–10	741–910	0.13	✓
Duan, Choudhari & Zhang (2016)	6	453.1	0.76	
Zhang, Duan & Choudhari (2017)	6	450	0.25, 0.76	
Zhang *et al.* (2018)	2.5–14	450–646	0.18–1.00	
Huang *et al.* (2020)	10.9, 13.64	617–1138	0.20	
Huang *et al.* (2022)	2.5, 4.9, 10.9	395–1199	0.20, 0.91, 1.00	
Lagha *et al.* (2011)	2.5–20	300–345	—	
Renzo & Urzay (2021)	10	140–1104	0.008	✓
Fu *et al.* (2021)	6	—	0.07	
Xu *et al.* (2021*a*)	8	1386, 2444	0.15, 0.80	
Xu *et al.* (2021*b*)	6, 8	688–2444	0.15, 0.4, 0.8	
Xu, Wang & Chen (2022)	6, 8	180–2391	0.15, 0.4, 0.8	
Cogo *et al.* (2022)	2, 5.86	520–1953	0.76	
Passiatore *et al.* (2021)	10	35-185	0.80	✓
Passiatore *et al.* (2022)	12.48	134–1128	—	✓
Zhang *et al.* (2022)	0.5, 2, 8	650	0.25, 0.5, 1.0	
Mo *et al.* (2023)	2.9, 7.25	340, 770	0.84, 1.0	
Li, Fu & Ma (2006)	6	265	0.94	
Li *et al.* (2022)	4.5	800	0.22	✓
Pirozzoli, Grasso & Gatski (2004)	2.25	—	1.00	
Liu *et al.* (2021)	2.25	1205	1.00	
Dong *et al.* (2022)	2.25	727.2–794.9	0.79, 1.58	

Table 1. Summary of DNS studies of supersonic and hypersonic turbulent boundary layers at different Mach numbers Ma, friction Reynolds numbers Re_τ and wall-to-recovery temperature ratios T_w/T_r in recent years. The '✓' indicates consideration of thermal or/and chemical non-equilibrium phenomena.

that uniform momentum spaces for the velocity and temperature fields exist in the high Reynolds number high-speed turbulent boundary layer.

Duan & Martín (2011) were the first to study the impact of high enthalpy effects on temporally evolving compressible turbulent boundary layers using DNS, and found that many scaling relations for low enthalpy boundary layers are still valid in high enthalpy boundary layers, and proposed a modified Crocco relation that is suitable for non-adiabatic cold walls and real gas effects. Subsequently, Passiatore *et al.* (2021) and Renzo & Urzay (2021) studied the effect of chemical non-equilibrium effects on the spatially evolving hypersonic boundary layer under quasi-adiabatic and wall-cooling conditions, respectively. Passiatore *et al.* (2022) further investigated the effect of thermochemical non-equilibrium effects on the wall-cooling spatially evolving hypersonic turbulent boundary layer. All of those studies reveal that the turbulence intensity and the fluctuations of thermodynamic quantities in the near-wall region of the hypersonic turbulent boundary layer are intensified at high Mach numbers and low wall temperatures. These findings suggest an enhancement in the compressibility of the turbulent boundary layer.

According to the Stokes assumption, the bulk viscosity coefficient in the Navier–Stokes equation is typically considered small compared to the shear viscosity coefficient, allowing it to be ignored in most numerical solutions of the Navier–Stokes equation

(Stokes 1851). However, this assumption does not hold for highly compressible fluids or polyatomic molecules with significant internal energy excitation. In such cases, the effect of bulk viscosity becomes non-negligible. Particularly in the context of the hypersonic compressible turbulent boundary layer, where strong compressibility is a defining characteristic, the impact of bulk viscosity becomes notably important. Under these conditions, accounting for bulk viscosity is crucial for capturing accurately the behaviour and characteristics of the turbulent boundary layer in hypersonic flows.

More precisely, the viscous stress τ_{ij} with bulk viscosity in momentum equation is expressed as

$$\tau_{ij} = 2\mu S_{ij}^{(d)} + \mu_b u_{k,k}\delta_{ij}, \tag{1.1}$$

where μ is the shear viscosity coefficient, μ_b is the bulk viscosity coefficient, $S_{ij}^{(d)} = S_{ij} - u_{k,k}\delta_{ij}/3$ represents the deviatoric part of the strain rate tensor, S_{ij} denotes the strain rate tensor, $u_{k,k}$ denotes the velocity divergence, and δ_{ij} is the Kronecker symbol. Then the related viscous dissipation is expressed as (Lele 1994)

$$\Phi = \tau_{ij}S_{ij} = 2\mu S_{ij}^{(d)} S_{ij}^{(d)} + \mu_b u_{k,k}^2, \tag{1.2}$$

where $2\mu S_{ij}^{(d)} S_{ij}^{(d)}$ is the shear dissipation, and $\mu_b u_{k,k}^2$ is the dilatational dissipation. The dilatational dissipation is small compared to the shear dissipation, but many studies have shown that dilatational dissipation plays an important role in compressible turbulence, which is closely related to bulk viscosity (Sarkar *et al.* 1991; Lele 1994; Zhu *et al.* 2016).

Furthermore, the total stress can be expressed as

$$\sigma_{ij} = -p\delta_{ij} + 2\mu S_{ij}^{(d)} + \mu_b u_{k,k}\delta_{ij}, \tag{1.3}$$

according to the definition of mechanical pressure $p_m = -\sigma_{ii}/3$, using the above equation, the relation between mechanical pressure and thermodynamic pressure can be obtained as

$$p_m = p - \mu_b u_{k,k}, \tag{1.4}$$

where the mechanical pressure is related to the translational energy of gas molecules, and the thermodynamic pressure corresponds typically to the internal energy of molecules, including molecular translational, rotational and vibrational energies of diatomic and polyatomic gases. Classically, the bulk viscosity is employed to characterize relaxation phenomena of these energy modes, noting that the non-zero bulk viscosity of monatomic gases was reported in the literature (DeGottardi & Matveev 2023; Sharma, Pareek & Kumar 2023), but very small. In the near-wall region of the hypersonic turbulent boundary layer, the effects of compression or dilatation are particularly significant, leading to intensified fluctuations of thermodynamic quantities. The rapid changes in the thermodynamic state of the gas give rise to non-equilibrium phenomena of energy in this region. The role of bulk viscosity becomes crucial in the re-equilibrium process of energy, underscoring its significance in the hypersonic turbulent boundary layer.

The bulk viscosity of a fluid can be determined by experimental, theoretical and numerical methods. As shown in table 2, the experimental methods include mainly acoustic wave absorption and dispersion experiments, and Rayleigh–Brillouin scattering experiments (Eu & Ohr 2001; Vieitez *et al.* 2010). The acoustic absorption and scattering experiments and Rayleigh–Brillouin scattering experiments measure the bulk viscosity at different frequencies, which leads to a significant difference in the bulk viscosity coefficients obtained from the two methods (Prangsma, Alberga & Beenakker 1973; Pan,

	Method	T_g (K)	N_2	O_2	CO_2		
Prangsma *et al.* (1973)	SA	293	0.73	—	—	0.78 (CO)	1.33 (CH_4)
Eu & Ohr (2001)	SA	293	0.8	—	—	34.93 (H_2)	22 (D_2)
Pan, Shneider & Miles (2004)	CRBS	292	0.73	0.4	1000		
Pan *et al.* (2005)	CRBS	292	—	—	0.4		
Vieitez *et al.* (2010)	CRBS	293	1.47	1.48	—	0.4 (CO_2–He)	
Vieitez *et al.* (2010)	SRBS	293	1.24	1.29	—		
Gu & Ubachs (2014)	SRBC	339.9	1.06	1.20	—		

Table 2. The bulk-to-shear viscosity ratios (μ_b/μ) of different gases determined by experimental methods. In the table, SA denotes acoustic absorption method, and CRBS and SRBS indicate coherent and spontaneous Rayleigh–Brillouin scattering, respectively. Also, T_g denotes the temperature of the gas during the experimental measurements.

Shneider & Miles 2005). In the area of theoretical research, Tisza (1942) investigated the bulk viscosity coefficient of an ideal gas by theoretical methods and concluded that the bulk-to-shear viscosity ratio of CO_2 gas at room temperature and pressure is of the order of 10^3. Zuckerwar & Ash (2006) developed an analytical formulation with multiple dissipative processes based on the variational principle of Hamilton, and found that the bulk-to-shear viscosity ratio of air is greater than 1.6×10^4. Subsequently, Cramer (2012) studied the variation of bulk viscosity with temperature and pressure for a variety of gases, and found that the bulk viscosities for a variety of fluids, including common polyatomic gases, are hundreds or thousands of times higher than the shear viscosity. However, Kustova, Mekhonoshina & Kosareva (2019) proposed a new bulk viscosity theory using the Chapman–Enskog method, which suggests that the CO_2 bulk viscosity and shear viscosity coefficients are of the same order at room temperature. In addition, many researchers have developed different theoretical models that include temperature-dependent bulk viscosity in recent years, such as the variable specific heat two-temperature Navier–Stokes equation (Kosuge & Aoki 2022), a state-to-state model suitable for mixtures of gases (Bruno & Giovangigli 2022), and a kinetic model with temperature-dependent vibrational degrees of freedom (Li & Wu 2022). Despite the many methods of evaluating the bulk viscosity coefficients, there are still large uncertainties in the bulk viscosity coefficients of common gases such as air, N_2 and CO_2 (Graves & Argrow 1999; Vieitez *et al.* 2010; Jaeger, Matar & Müller 2018; Sharma & Kumar 2023). The Navier–Stokes equation with a bulk viscosity term holds if the local thermodynamic equilibrium condition is satisfied (Vincenti & Kruger 1965). When the bulk viscosity is large, the maximum energy relaxation time of the molecules is much smaller than the time scale of the compressible turbulent boundary layer, and the local thermodynamic equilibrium condition is satisfied.

At present, research on the effect of bulk viscosity on compressible turbulence is relatively scarce, and the main focus is on the effect of bulk viscosity on compressible homogeneous isotropic turbulence (Liao, Peng & Luo 2009; Cramer & Bahmani 2014; Boukharfane *et al.* 2019; Touber 2019). Emanuel (1992) first studied the effect of bulk viscosity on hypersonic flow. The influence of bulk viscosity on the hypersonic laminar boundary layer at large Reynolds number is studied by presenting a first-order boundary layer equation including bulk viscosity at high Reynolds number. Pan & Johnsen (2017) studied the decay of compressible homogeneous isotropic turbulence using DNS in the bulk-to-shear viscosity ratio range 0–1000, investigating mainly the effect of bulk viscosity on turbulent kinetic energy dissipation. Chen *et al.* (2019) studied the effects of bulk

viscosity on Mach number scaling laws and small-scale structures of homogeneous isotropic turbulence and homogeneous shear turbulence with turbulent Mach numbers ranging from 0.1 to 0.6, and bulk-to-shear viscosity ratios 0, 10 and 30, using numerical simulation methods. However, no one has systematically investigated the effect of bulk viscosity on the hypersonic compressible turbulent boundary layer. Because of the strong compressibility of the hypersonic turbulent boundary layer and the rapid change of the thermodynamic state of the gas near the wall, bulk viscosity is of great significance in the study of the hypersonic turbulent boundary layer.

Based on the importance of bulk viscosity to the hypersonic compressible flat plate turbulent boundary layer and the relevant findings from DNS, this paper aims to investigate the effect of bulk-to-shear viscosity ratio $\mu_b/\mu = 100$ on the hypersonic compressible turbulent boundary layer using the DNS method. The rest of the paper is organized as follows. The governing equations, cases and parameters used in DNS are given in § 2. The statistics related to velocity are introduced in § 3, including transformed mean velocity profiles, Reynolds stresses and turbulent kinetic energy budgets. Section 4 presents the thermodynamic-related statistics, such as mean and fluctuating thermodynamic variables, strong Reynolds analogy and heat flux. Furthermore, the large-scale turbulent structures and small-scale properties are analysed in §§ 5 and 6, respectively. Additionally, the physical mechanism of the impact of bulk viscosity on turbulent boundary layers is discussed in § 7. Finally, the conclusions of this paper are summarized in § 8.

2. Numerical set-up

The three-dimensional compressible Navier–Stokes equations in conservation form of the calorimetrically perfect gas are

$$\frac{\partial \rho}{\partial t} + \frac{\partial (\rho u_j)}{\partial x_j} = 0, \tag{2.1}$$

$$\frac{\partial (\rho u_i)}{\partial t} + \frac{\partial (\rho u_i u_j + p\delta_{ij})}{\partial x_j} = \frac{\partial \sigma_{ij}}{\partial x_j}, \tag{2.2}$$

$$\frac{\partial E}{\partial t} + \frac{\partial [(E+p)u_j]}{\partial x_j} = \frac{\partial}{\partial x_j}\left(k\frac{\partial T}{\partial x_j}\right) + \frac{\partial (\sigma_{ij}u_i)}{\partial x_j}, \tag{2.3}$$

where $i, j = x, y, z$ represent streamwise, wall-normal and spanwise coordinates, respectively. Here, ρ is density, u_j represents velocity in three directions, and p is the thermodynamic pressure. Also, $E = p/(\gamma - 1) + 1/2\rho u_k u_k$ denotes total energy per unit volume, where $\gamma = 1.4$, and $k = c_p\mu/Pr$ is the thermal conductivity coefficient, with Prandtl number $Pr = 0.7$ and shear viscosity coefficient μ. When the effect of bulk viscosity is considered, the viscous stress tensor σ_{ij} is expressed as

$$\sigma_{ij} = \mu\left(\frac{\partial u_i}{\partial x_j} + \frac{\partial u_j}{\partial x_i} - \frac{2}{3}\frac{\partial u_k}{\partial x_k}\delta_{ij}\right) + \mu_b\frac{\partial u_k}{\partial x_k}\delta_{ij}, \tag{2.4}$$

where μ_b denotes the bulk viscosity coefficient.

The compressible Navier–Stokes equations are solved by the high-order finite-difference method (Hou *et al.* 2023). A hybrid scheme of sixth-order central finite difference combined with a fifth-order weighted essentially non-oscillatory method (Jiang & Shu 1996) is used for the convective terms to ensure that shock-capturing can be performed and to ensure the stability of the numerical simulation, and sixth-order central finite

Case	Ma_∞	U_∞ (m s^{-1})	ρ_∞ (kg m^{-3})	T_∞ (K)	T_w (K)	T_w/T_r	Re_τ	Re_τ^*	Re_∞	μ_b/μ
$Ma6T_w0.76$	5.86	870.4	0.043	55	300	0.76	453	5390	226 838	0
$Ma6T_w0.76\mu_b$	5.86	870.4	0.043	55	300	0.76	453	5390	226 838	100
$Ma8T_w0.48$	7.87	1155.1	0.026	51.8	298	0.48	480	6380	294 966	0
$Ma8T_w0.48\mu_b$	7.87	1155.1	0.026	51.8	298	0.48	480	6380	294 966	100
$Ma6T_w0.25$	5.84	869.1	0.044	55.2	97.5	0.25	450	1121	35 972	0
$Ma6T_w0.25\mu_b$	5.84	869.1	0.044	55.2	97.5	0.25	450	1121	35 972	100

Table 3. The cases and parameters of DNS. The parameters with symbol ∞ refer to the inflow parameters. The parameters with subscript w indicate the wall parameters. The parameters with subscript r refer to the recovery parameters. Here, $Re_\tau = \rho_w u_\tau \delta/\mu_w$ is the friction Reynolds number, $Re_\tau^* = \sqrt{\rho_\infty \tau_w}\,\delta/\mu_\infty$ is the semi-local friction Reynolds number, $Re_\infty = \rho_\infty u_\infty \delta/\mu_\infty$ is the inflow Reynolds number, and μ_b is the bulk viscosity coefficient.

difference is used for the viscous terms. The system is advanced in time using a third-order Runge–Kutta scheme. Inflow turbulence boundary conditions are established by the digital filtering method, non-reflecting boundary conditions for the upper boundary and outflow, no-slip isothermal boundary conditions for the wall, and periodic boundary conditions for the spanwise direction, where the fluid is considered to be statistically homogeneous.

To investigate the influence of bulk viscosity on the hypersonic compressible turbulent boundary layer, six cases are selected carefully for DNS, as shown in table 3. Using the base case with parameters $Ma6T_w0.76$, the impact of wall cooling is analysed systematically by comparing the results with those of $Ma6T_w0.25$. Additionally, the effect of Mach number is investigated by comparing the results with those of $Ma8T_w0.48$. Numerous studies have been conducted for the cases where the bulk-to-shear viscosity coefficient ratio is 0 ($\mu_b/\mu = 0$). Due to the uncertainty of the bulk viscosity coefficient (Vieitez *et al.* 2010; Kustova *et al.* 2019) and the impact of the large bulk viscosity coefficient ($\mu_b/\mu = O(Re^{1/2})$) on the boundary layer (Cramer & Bahmani 2014), the bulk-to-shear viscosity coefficient ratios μ_b/μ are chosen as 0 and 100, which are of the same magnitude as the square root of inflow Reynolds number ($Re_\infty^{1/2}$). Building upon this established foundation, the DNS are performed on the corresponding cases where the bulk viscosity ($\mu_b/\mu = 100$) is taken into account. In summary, this paper investigates $Ma6T_w0.76$, $Ma8T_w0.48$ and $Ma6T_w0.25$, with and without bulk viscosity, for a total of six DNS cases.

The main parameters required for DNS are also shown in table 3, including Mach number Ma_∞, velocity U_∞, density ρ_∞, temperature T_∞ and T_w, where ∞ denotes the inflow value and w denotes the value at the wall. Also, T_w/T_r is the temperature ratio, where $T_r = T_\infty(1 + 0.5r(\gamma - 1)\,Ma_\infty^2)$ denotes the recovery temperature, and $r = 0.89$ is the recovery factor. The friction Reynolds number is defined as $Re_\tau = \rho_w u_\tau \delta/\mu_w$, where $u_\tau = \sqrt{\tau_w/\rho_w}$ is the friction velocity, $\tau_w = \mu(\partial u/\partial y)$ represents the shear stress at the wall, δ is the boundary layer thickness based on 99 % of the inflow velocity, and the dynamic viscosity coefficient μ is calculated using the Sutherland formula $\mu = T^{3/2}(1 + 110.4/T_\infty)/(T + 110.4/T_\infty)$. Also, $Re_\tau^* = \rho_\infty\sqrt{\tau_w/\rho_\infty}\,\delta/\mu_\infty$ is the semi-local friction Reynolds number, and $Re_\infty = \rho_\infty u_\infty \delta/\mu_\infty$ is the inflow Reynolds number.

In order to ensure that the DNS results remain unaffected by the inflow conditions, a sufficiently long streamwise computational domain is employed. Additionally, to capture accurately the small-scale structures in the near-wall region within the boundary layer,

Case	L_x/δ_i	L_y/δ_i	L_z/δ_i	Δx^+	Δy^+_{min}	Δz^+	N_x	N_y	N_z
$Ma6T_w0.76$	50	15	3.84	11.1	0.8	6.8	2048	384	256
$Ma6T_w0.76\mu_b$	50	15	3.84	11.1	0.8	6.8	2048	384	256
$Ma8T_w0.48$	50	10	6	9.6	0.55	11.5	2500	450	250
$Ma8T_w0.48\mu_b$	50	8	6	9.6	0.55	11.5	2500	450	250
$Ma6T_w0.25$	33	8	3.2	6.2	0.46	3.6	2400	320	400
$Ma6T_w0.25\mu_b$	33	8	3.2	6.2	0.46	3.6	2400	320	400

Table 4. The parameters of the computational domain and mesh. Here, δ_i is the inflow boundary layer thickness. The subscripts x, y and z represent the streamwise, wall-normal and spanwise directions, respectively.

a stretched grid is used in the wall-normal direction, where a minimum grid height $\Delta y^+_{\min}$ equals 0.46 in the first layer of grid. The streamwise and spanwise directions, however, utilize a uniform grid. The computational domain ($L_x \times L_y \times L_z$), grid size ($\Delta x^+ \times \Delta y^+ \times \Delta z^+$) and number of grids ($N_x \times N_y \times N_z$) are shown in table 4, where the superscript + indicates the inner scaling, $y^+ = y/y_\tau$, $u^+ = u/u_\tau$, with $y_\tau = \nu_w/u_\tau$ and $\nu_w = \mu_w/\rho_w$.

Figure 1 displays the outcomes of the van Driest transformed mean velocity, the root mean square (r.m.s.) streamwise, wall-normal and spanwise velocity fluctuations and Reynolds shear stress, the r.m.s. density fluctuations, and the r.m.s. temperature fluctuations, which are compared with the corresponding results from Zhang *et al.* (2018). The excellent agreement observed in the figure demonstrates that the physical setting and numerical tool employed in this study can successfully achieve the required accuracy for DNS.

It is worth noting here that both standard Reynolds averages and density-weighted (Favre) averages are utilized to characterize turbulence statistics. For a variable f, the mean component of the Reynolds averages is denoted as $\bar{f}$, and the fluctuating component is represented by f'. Consequently, the variable f can be expressed as $f = \bar{f} + f'$. On the other hand, the mean component of the Favre average is denoted as $\tilde{f}$, and the fluctuating component is indicated by f''. The Favre average is computed as $\tilde{f} = \overline{\rho f}/\bar{\rho}$, where $\overline{\rho f}$ represents the density-weighted average of the variable f, and $\bar{\rho}$ denotes the mean density. Hence the variable f can be expressed as $f = \tilde{f} + f''$.

3. Velocity-related statistics

3.1. *Transformed mean velocity profiles*

To investigate the effect of compressibility on the mean velocity profiles of compressible turbulent channels, pipes and boundary layers at high Mach numbers and/or low wall temperatures, various transformed mean velocity profiles have been proposed (Cheng *et al.* 2024). Through these approaches, the transformed mean velocity profiles are designed to collapse onto the incompressible laws. The incompressible laws are defined as

$$u^+ = y^+, \tag{3.1a}$$

$$u^+ = (1/k)\log(y^+) + C, \tag{3.1b}$$

where $k = 0.41$ and $C = 5.2$.

One of the most classical and widely used mean velocity transformations was proposed by van Driest based on the Morkovin assumption (van Dreist 1956; Morkovin 1962).

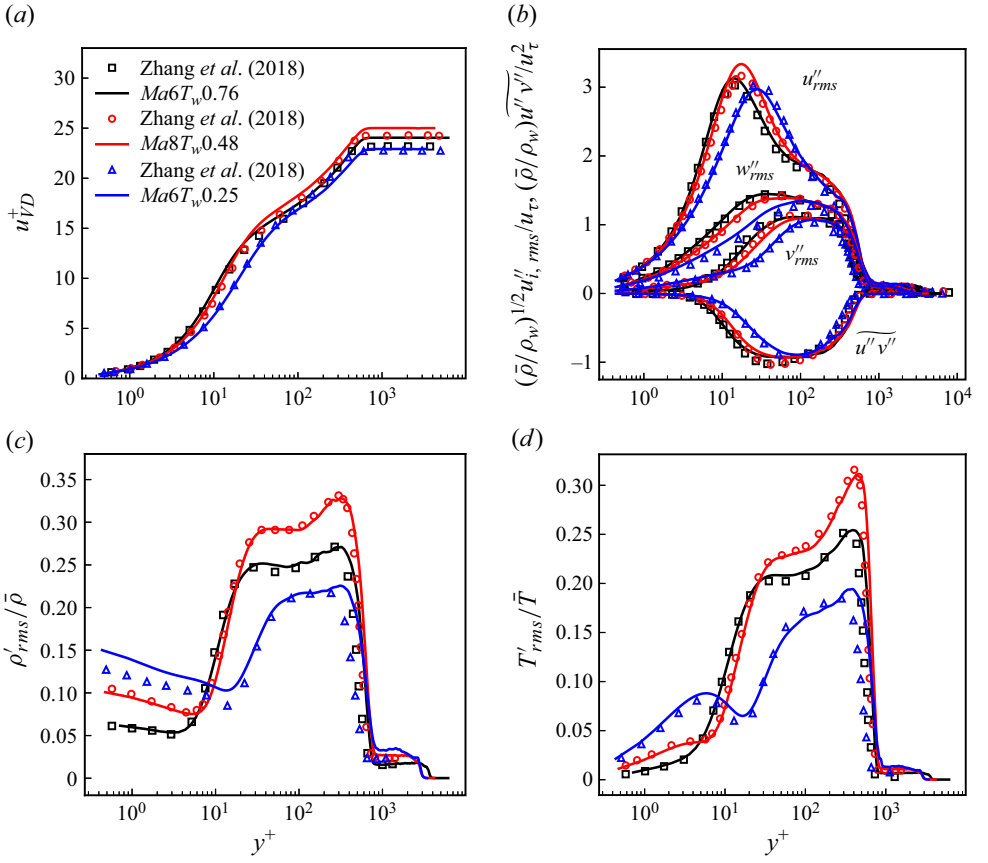

Figure 1. Comparison between the DNS results without considering bulk viscosity and the results of Zhang *et al.* (2018). Variation of (*a*) the van Driest (VD) transformed mean velocity, (*b*) the r.m.s. velocity fluctuations and Reynolds shear stress, (*c*) the r.m.s. density fluctuations, and (*d*) the r.m.s. temperature fluctuations along the wall-normal distance in the inner scaling.

Its definition is

$$u_{VD}^{+} = \int_0^{u^+} (\bar{\rho}/\bar{\rho}_w)^{1/2}\,\mathrm{d}\tilde{u}^{+}. \tag{3.2}$$

To improve the performance of the van Driest transformation under the wall-cooling condition, Trettel & Larsson (2016) proposed a new form of mean velocity transformation based on the log law and the conservation of near-wall momentum, which is defined as

$$u_{TL}^{+} = \int_0^{u^+} \sqrt{\frac{\bar{\rho}}{\rho_w}}\left[1 + \frac{1}{2}\frac{1}{\bar{\rho}}\frac{\mathrm{d}\bar{\rho}}{\mathrm{d}y}\,y - \frac{1}{\bar{\mu}}\frac{\mathrm{d}\bar{\mu}}{\mathrm{d}y}\,y\right]\mathrm{d}\tilde{u}^{+}, \tag{3.3a}$$

$$y^{*} = \frac{\bar{\rho}(\tau_w/\bar{\rho})^{1/2}y}{\bar{\mu}}. \tag{3.3b}$$

This transformation can make the transformed mean velocity profiles collapse well with the incompressible linear law in the viscous sublayer and the buffer layer, while in the log region, it deviates significantly from the incompressible log law.

Therefore, Volpiani *et al.* (2020) proposed a new mean velocity transformation suitable for non-adiabatic wall turbulence by further analysing the universality in the viscous sublayer and Morkovin-scaled shear stress, and combining data-driven methods to determine the non-dimensionalizations, which are defined as

$$u_V^+ = \int_0^{u^+} \frac{(\bar{\rho}/\rho_w)^{1/2}}{(\bar{\mu}/\mu_w)^{1/2}}\,\mathrm{d}\bar{u}^+, \tag{3.4a}$$

$$y_V^+ = \int_0^{y^+} \frac{(\bar{\rho}/\rho_w)^{1/2}}{(\bar{\mu}/\mu_w)^{3/2}}\,\mathrm{d}\bar{y}^+. \tag{3.4b}$$

Recently, Griffin, Fu & Moin (2021) scaled the viscous stress using the semi-local scaling in the viscous sublayer, and analysed the Reynolds stress based on the principle of approximate equilibrium between the production term and dissipation term of turbulent kinetic energy in the log layer. They further proposed a velocity-transformed form based on the total stress equation

$$u_{TS}^+ = \int_0^{y^*} \frac{\tau^+ S_{eq}^+}{\tau^+ + S_{eq}^+ - S_{TL}^+}\,\mathrm{d}y^*, \tag{3.5}$$

where $\tau^+ = \tau_v^+ + \tau_R^+$ is total stress, while $\tau_v^+ = (\mu \partial u/\partial y)/\tau_w$ and $\tau_R^+ = (-\bar{\rho}\widetilde{u''v''})/\tau_w$ are the scaled viscous and Reynolds shear stresses, respectively. Here, $S_{TL}^+ = (\bar{\mu}/\mu_w)(\partial u^+/\partial y^+)$ and $S_{eq}^+ = (\mu_w/\bar{\mu})(\partial u^+/\partial y^*)$ are the generalized non-dimensional mean shear stresses derived for the viscous sublayer and the log layer, respectively, and y^* is the wall-normal coordinate in the semi-local scaling (Huang, Coleman & Bradshaw 1995). The semi-local scaling is defined as $y^* = y/y_\tau^*$, where $y_\tau^* = \bar{\mu}/(\bar{\rho}\tau_w)^{1/2}$.

Figure 2 presents the transformed mean velocity profiles u_{VD}^+, u_{TL}^+, u_V^+ and u_{TS}^+ at two different bulk-to-shear viscosity ratios for each case of the DNS. The van Driest transformed mean velocity profile u_{VD}^+ adheres to an incompressible linear law only in the region very close to the wall in the wall-cooling cases. This behaviour is attributed to the increased gradient of relevant parameters in the near-wall region and the rapid changes in mean density and viscosity coefficient in the viscous sublayer. The Trettel and Larsson transformation u_{TL}^+ can make the mean velocity profiles of the compressible turbulent boundary layer with low wall temperature similar to the incompressible linear law in the viscous sublayer, but both the van Driest transformation u_{VD}^+ and Trettel and Larsson transformation u_{TL}^+ are significantly different from the incompressible log law in the log region. Xu *et al.* (2021*b*), Zhang *et al.* (2022) and Huang *et al.* (2022) have respectively reached similar conclusions. In contrast, the Volpiani velocity transformation u_V^+ based on physical analysis and data driven by Volpiani *et al.* (2020) and the total-stress-based mean velocity transformation u_{TS}^+ by Griffin *et al.* (2021) can collapse the mean velocity profiles of the compressible turbulent boundary layer with high Mach number and low wall temperature to the incompressible laws of the wall in the viscous sublayer, buffer layer and log layer, which is consistent with the results of Huang *et al.* (2022) and Cogo *et al.* (2022). Additionally, as the Mach number increases and the wall temperature decreases, the Volpiani velocity transformation u_V^+ and the total-stress-based mean velocity transformation u_{TS}^+ collapse better with the incompressible scaling laws in the log region by considering the bulk viscosity, indicating that bulk viscosity makes the production term and dissipation term of turbulent kinetic energy more balanced in the log region. However, the transformed mean velocity profiles considering bulk viscosity show no

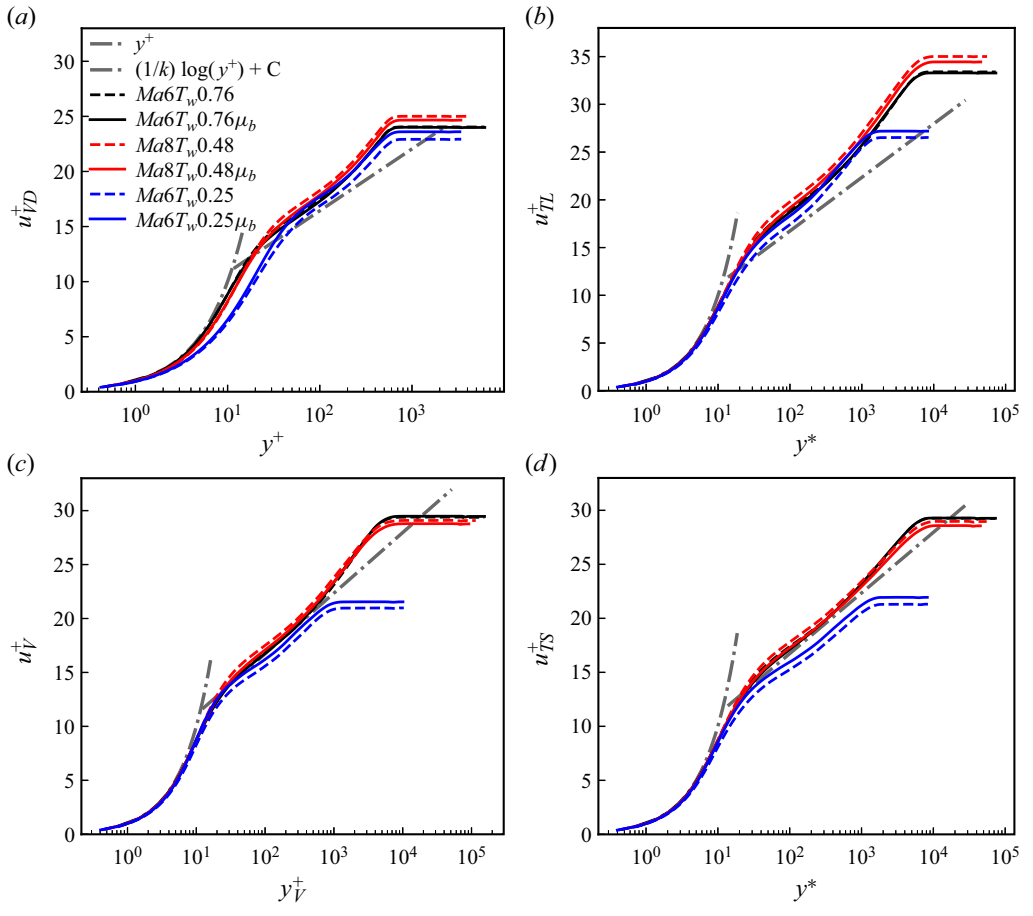

Figure 2. Transformed mean velocity profiles: (*a*) the van Driest transformation; (*b*) the Trettel and Larsson transformation; (*c*) the data-driven-based transformation of Volpiani *et al.*; and (*d*) the total-stress-based transformation of Griffin *et al.* The results are compared with linear law $u^+ = y^+$ and log law $u^+ = (1/k)\log(y^+) + C$, where $k = 0.41$, $C = 5.2$ in (*a*), and $k = 0.41$, $C = 5.5$ in (*b*), (*c*) and (*d*).

significant differences compared to those without bulk viscosity, closely resembling the incompressible results. This observation indicates that bulk viscosity has minimal effect on the compressible transformed mean velocity profiles.

3.2. *Fluctuations of velocity*

Figure 3 shows the variation of the turbulence intensities in the streamwise, wall-normal and spanwise directions using the Morkovin transformation (Morkovin 1962) with wall-normal distance in inner scaling (y^+) and semi-local scaling (y^*), respectively. Figure 4 displays the variation of Reynolds shear stress with the wall-normal distance in inner scaling and semi-local scaling, respectively. It is worth noting that the streamwise (u''_{rms}), wall-normal (v''_{rms}) and spanwise (w''_{rms}) r.m.s. velocity fluctuations exhibit better similarity in the outer boundary layer than those in the inner layer for cases with different Mach numbers and wall temperature conditions in the inner scaling. Conversely, in the semi-local scaling, the turbulence intensities in the three directions for cases with different inflow conditions collapse well in the viscous sublayer and log layer. These findings are

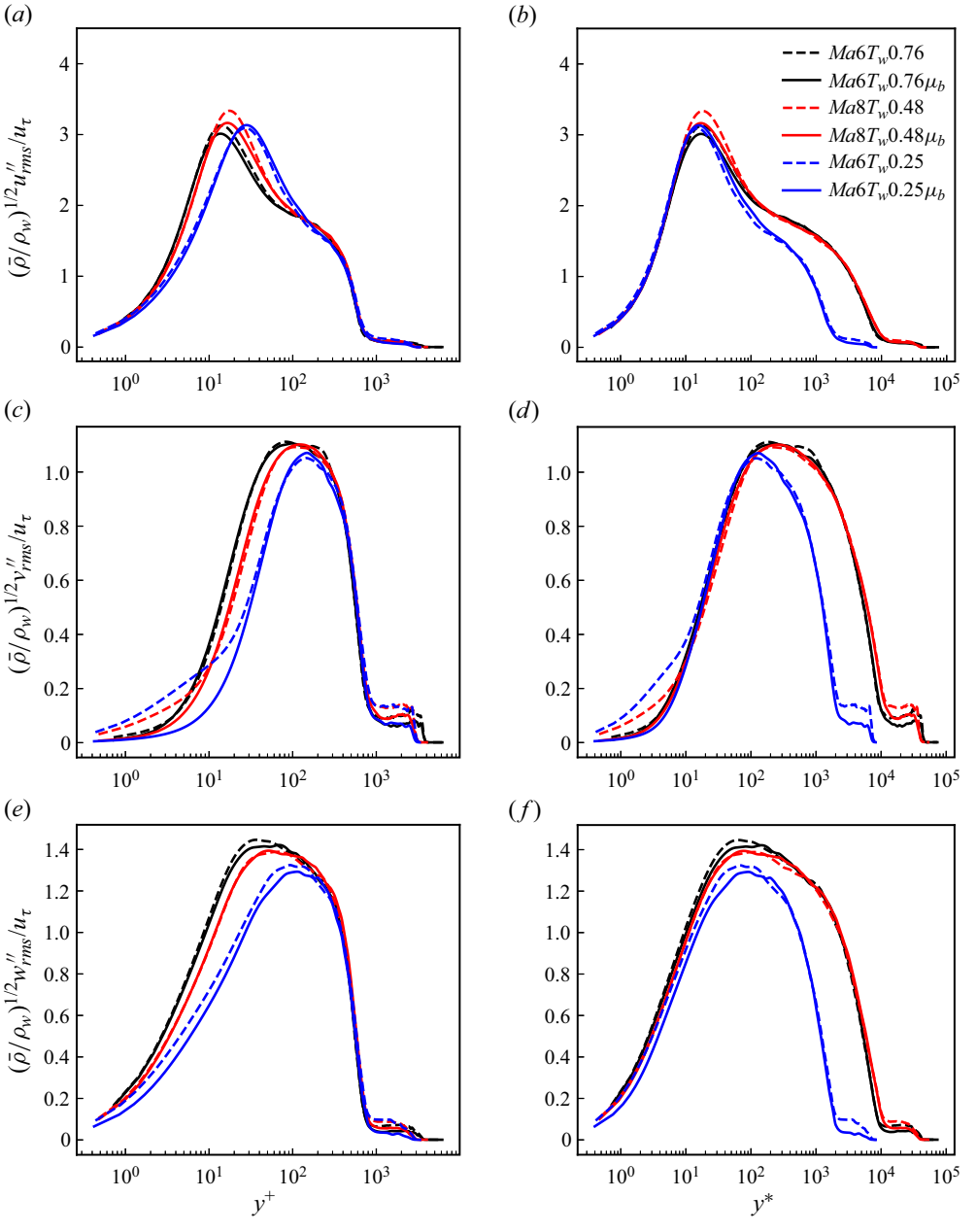

Figure 3. Streamwise, wall-normal and spanwise turbulence intensities scaled according to the Morkovin transformation in (*a*,*c*,*e*) the inner scaling, and (*b*,*d*,*f*) the semi-local scaling.

consistent with previous studies by Zhang *et al.* (2018) and Cogo *et al.* (2022). In addition, the peak of turbulence intensities in the streamwise, wall-normal and spanwise directions of different cases can have a better collapse by considering the variation of the mean density, which proves the validity of the Morkovin transformation (Morkovin 1962). A similar trend can be found in the Reynolds shear stress in figure 4. As shown in the figures, after considering the bulk viscosity, the r.m.s. wall-normal velocity fluctuations decrease in the viscous sublayer because of the increase of the dilatational dissipation. And as shown

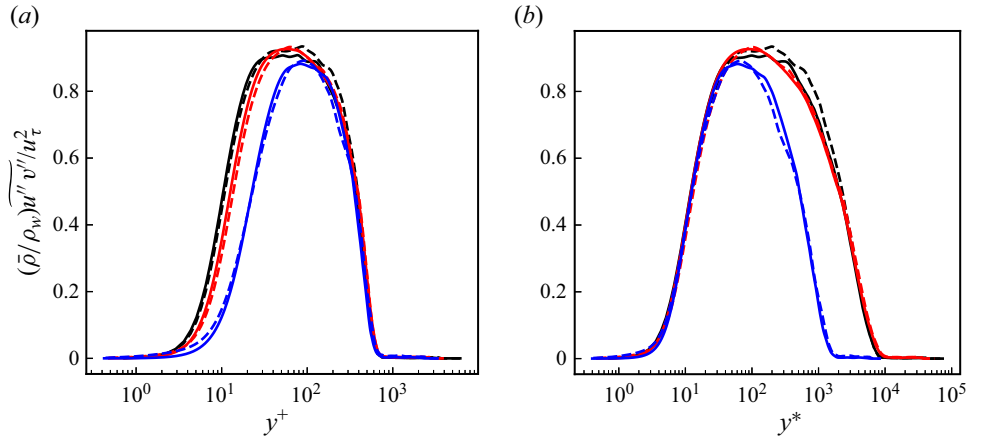

Figure 4. Reynolds shear stress scaled by the Morkovin transformation in the (*a*) inner scaling and (*b*) semi-local scaling.

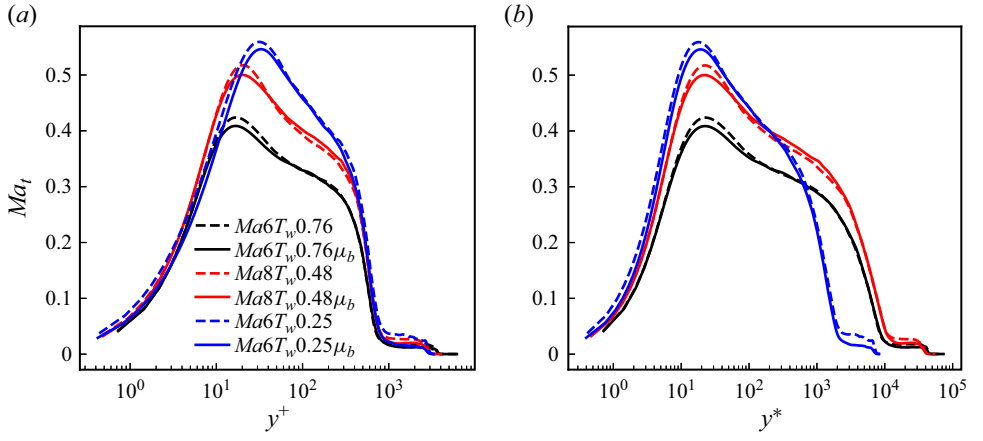

Figure 5. Turbulent Mach number for different cases in (*a*) the inner scaling, and (*b*) the semi-local scaling.

in figure 4, the bulk viscosity causes the Reynolds shear stress to decrease slightly in the log layer.

Figure 5 shows the turbulent Mach number for different cases in the inner scaling and semi-local scaling, respectively. It can be seen that the bulk viscosity slightly reduces the peak value of turbulent Mach number Ma_t, indicating that the bulk viscosity weakens the compressibility effects of the hypersonic turbulent boundary layer. The maximum value of the turbulent Mach number increases as the Mach number increases and the wall temperature decreases, in agreement with the results of Duan *et al.* (2010), Lagha *et al.* (2011) and Zhang *et al.* (2022).

3.3. *Turbulent kinetic energy budget*

Turbulent kinetic energy is analysed to quantify the influence of the bulk viscous term on the hypersonic boundary layer turbulence flow, which is commonly used to characterize the fluctuating motion of a fluid per unit mass and is defined as

$$\tilde{k} = \frac{1}{2}\frac{\overline{\rho u_k'' u_k''}}{\bar{\rho}}. \tag{3.6}$$

The budget equation of turbulent kinetic energy is

$$\frac{\partial(\bar{\rho}\tilde{k})}{\partial t}+\frac{\partial(\bar{\rho}\tilde{k}\widetilde{u}_j)}{\partial x_j}=P+T+\Pi+\Phi_{dif}+\Phi_{dis}+ST, \tag{3.7}$$

where

$$P=-\overline{\rho u_i'' v''}\,\frac{\partial\widetilde{u}_i}{\partial y}, \tag{3.8}$$

$$T=-\frac{1}{2}\frac{\partial}{\partial y}\overline{\rho u_i'' u_i'' v''}, \tag{3.9}$$

$$\Pi=\Pi_t+\Pi_d=-\frac{\partial}{\partial y}\overline{v''p'}+\overline{p'\frac{\partial u_i''}{\partial x_i}}, \tag{3.10}$$

$$\Phi_{dif}=\frac{\partial}{\partial y}\overline{u_i''\sigma_{iy}'}, \tag{3.11}$$

$$\Phi_{dis}=-\overline{\sigma_{ij}'\frac{\partial u_i''}{\partial x_j}}, \tag{3.12}$$

$$ST=-\overline{v''}\,\frac{\partial\bar{p}}{\partial y}+\overline{u_i''}\,\frac{\partial\overline{\sigma_{ij}}}{\partial x_j}-\bar{\rho}\tilde{k}\,\frac{\partial\tilde{v}}{\partial y}. \tag{3.13}$$

The physical significance of each term in the turbulent kinetic energy budget equation is: P is the production term of turbulent kinetic energy, which characterizes the energy input from Reynolds stress to the turbulent fluctuating motion through the deformation rate of the mean motion; T denotes the turbulent diffusion term, which characterizes the diffusion of turbulent kinetic energy generated by the fluctuating motion; Π includes the pressure diffusion term and pressure dilatation term, where Π_t is the pressure diffusion term, and Π_d is the pressure dilatation term; Φ_{dif} represents the viscous diffusion term, which characterizes the spatial transport of turbulent kinetic energy due to the viscous stress; and Φ_{dis} denotes the viscous dissipation term, which represents the viscous dissipation due to the turbulent fluctuating motion.

Figures 6(*a–c*) present the budget terms of turbulent kinetic energy normalized by the conventional inner scaling, and figure 6(*d*) shows the turbulent kinetic energy transport in the semi-local scaling. Compared to the inner scaling, the turbulent kinetic energy transport in semi-local scaling for different Mach numbers and wall temperature conditions collapses better, which is consistent with the results of Duan *et al.* (2011) and Zhang *et al.* (2018). In addition, the ratio of the turbulent kinetic energy production term P to the viscous dissipation term Φ_{dis} in the log layer is greater than 1 in the semi-local scaling, while the ratio of the turbulent kinetic energy production term P to the sum of the viscous dissipation term Φ_{dis} and the turbulent diffusion term T is approximately 1, which is consistent with the findings of Pirozzoli *et al.* (2021) and Cogo *et al.* (2022). As shown in the figures, the bulk viscosity significantly reduces the pressure diffusion term Π_t and pressure dilatation term Π_d near the wall. The wall-normal velocity fluctuations in the pressure diffusion term are much smaller than the pressure fluctuations, so the pressure diffusion term Π_t near the wall is determined by the gradient of the wall-normal velocity fluctuations. And the bulk viscosity will significantly reduce the gradient of the wall-normal velocity fluctuations near the wall, as shown in figures 3(*c*) and 3(*d*). Therefore, the pressure diffusion term Π_t near the wall experiences a notable reduction.

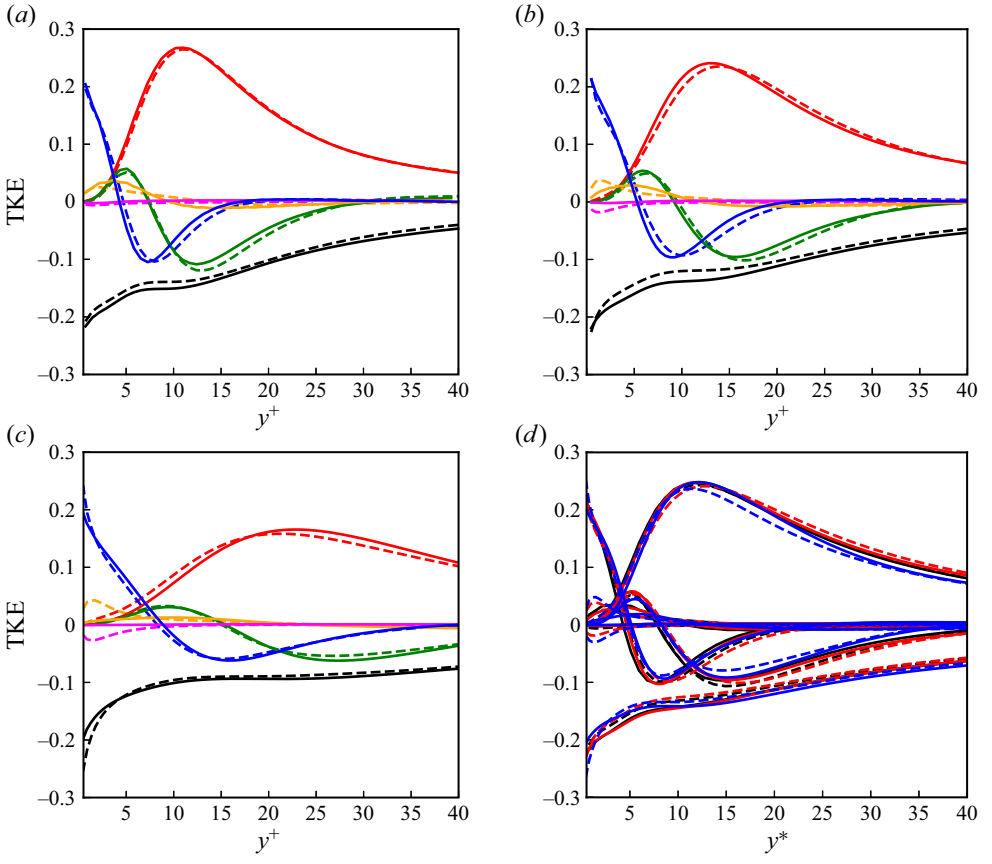

Figure 6. Turbulent kinetic energy (TKE) budget. Wall-normal distribution of (*a*) $Ma6T_w0.76$, (*b*) $Ma8T_w0.48$ and (*c*) $Ma6T_w0.25$ with (solid lines) and without (dashed lines) bulk viscosity in inner scaling, and (*d*) turbulent kinetic energy budget for different cases in semi-local scaling. The turbulent kinetic energy budget consists of the production P (red lines), turbulent diffusion T (green lines), pressure diffusion Π_t (orange lines), pressure dilatation Π_d (magenta lines), viscous diffusion Φ_{dif} (blue lines) and viscous dissipation Φ_{dis} (black lines) in (*a–c*). Plot (*d*) consists of the turbulent kinetic energy budget of $Ma6T_w0.76$ (black lines), $Ma8T_w0.48$ (red lines) and $Ma6T_w0.25$ (blue lines) with and without bulk viscosity. Solid lines are for $\mu_b/\mu = 100$; dashed lines are for $\mu_b/\mu = 0$.

Similarly, the pressure dilatation term Π_d represents the influence of the fluctuating density generated by the compressibility effect on the growth rate of turbulent kinetic energy. The presence of bulk viscosity causes a decrease in fluid compressibility and density fluctuations near the wall, resulting in a significant reduction of the pressure dilatation term Π_d.

4. Thermodynamic-related statistics

4.1. *Mean thermodynamic statistics*

Figure 7 displays mean density and mean temperature for different cases. The mean density and mean temperature considering the bulk viscosity are in good agreement with the results without considering bulk viscosity, so the influence of bulk viscosity on the mean density and mean temperature can be ignored. The effects of Mach number and wall cooling on statistics, such as mean density, are consistent with the results of Duan *et al.* (2010) and Zhang *et al.* (2022). As the wall-normal distance increases, the mean

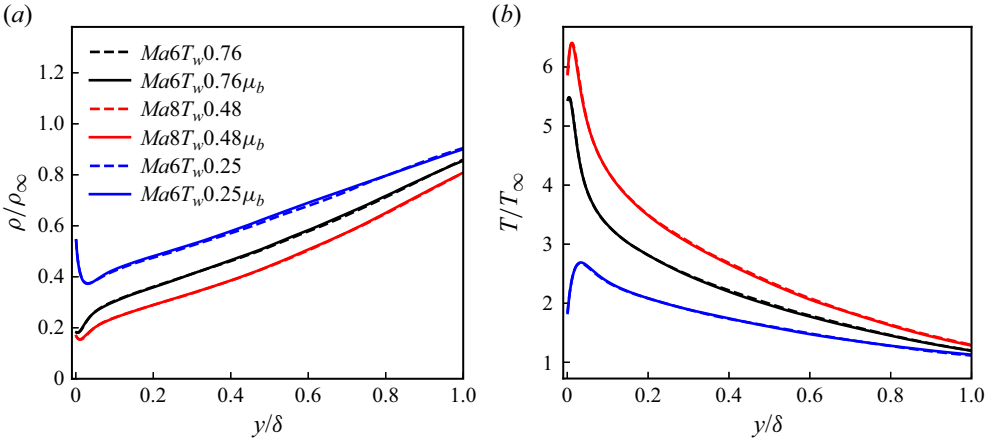

Figure 7. Wall-normal distributions of (*a*) mean density and (*b*) mean temperature in outer scaling.

density in the boundary layer decreases slightly in the viscous sublayer, then increases linearly. The mean density continues to increase linearly in the log layer and the outer layer of the boundary layer with a slope smaller than that of the viscous sublayer. The mean temperature increases slightly in the near-wall region, and this phenomenon becomes more significant as the wall temperature decreases. As the Mach number increases, the velocity gradient near the wall increases, resulting in an increase in wall shear stress and an increase in temperature gradient near the wall. As the wall temperature decreases, the viscosity near the wall increases, and consequently, the temperature gradient near the wall also intensifies. However, with an increase in the wall-normal distance, the temperature gradient gradually decreases. Moreover, higher Mach numbers lead to an increase in the mean temperature within the boundary layer, while decreasing wall temperature results in a reduction of the mean temperature, causing the peak value of the mean temperature to move away from the wall.

Figure 8 plots the relation between mean temperature and mean velocity comparing with the Walz (1969) equation and the modified mean temperature–velocity relation of Zhang *et al.* (2014), respectively. The classical Walz (1969) equation is

$$\frac{T}{T_\infty} = \frac{T_w}{T_\infty} + \frac{T_r - T_w}{T_\infty}\left(\frac{u}{u_\infty}\right) + \frac{T_\infty - T_r}{T_\infty}\left(\frac{u}{u_\infty}\right)^2, \tag{4.1}$$

where T_w is wall temperature, $T_r = T_\infty(1 + 0.5r(\gamma - 1)Ma_\infty^2)$ denotes the recovery temperature, and $r = 0.89$ is the recovery factor.

Zhang *et al.* (2014) modified the relation between mean temperature and mean velocity by considering the variation of heat flux at the wall:

$$\frac{T}{T_\infty} = \frac{T_w}{T_\infty} + \frac{T_{rg} - T_w}{T_\infty}\left(\frac{u}{u_\infty}\right) + \frac{T_\infty - T_{rg}}{T_\infty}\left(\frac{u}{u_\infty}\right)^2, \tag{4.2}$$

where $T_{rg} = T_\infty + r_g u_\infty^2/2c_p$, $r_g = 2c_p(T_w - T_\infty)/u_\infty^2 - 2p_r q_w/(u_\infty \tau_w)$ and $q_w = -(k\,\partial T/\partial y)_w$.

As shown in the figure, the mean temperature–velocity relation modified by Zhang *et al.* (2014) is more accurate than that predicted by the Walz equation, especially as the Mach

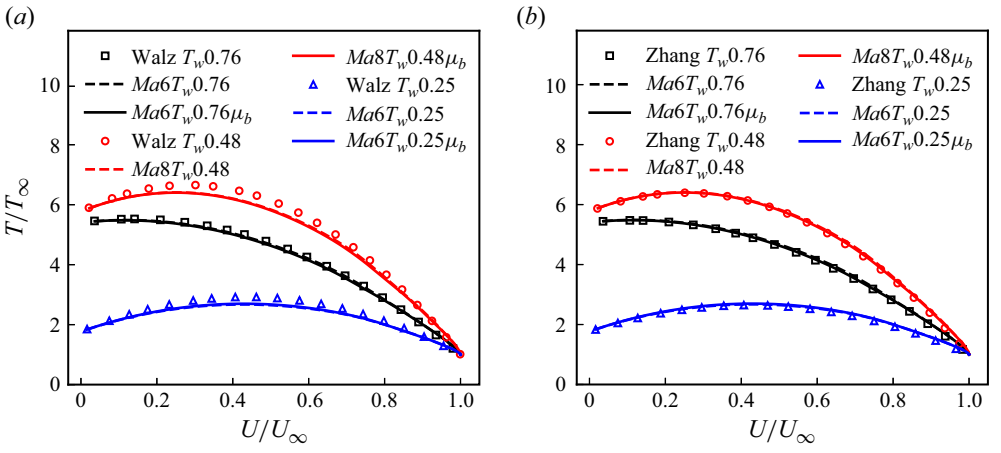

Figure 8. Relation between mean temperature and mean velocity: (*a*) equation of Walz (1969); (*b*) the modified equation proposed by Zhang *et al.* (2014). Symbols indicate theory results; lines indicate DNS results.

number increases and the wall temperature decreases, which is consistent with the results obtained by Zhang *et al.* (2018), Huang *et al.* (2022) and Cogo *et al.* (2022). However, the curves for $\mu_b/\mu = 0$ and $\mu_b/\mu = 100$ overlap approximately, indicating that bulk viscosity has almost no effect on the relation between mean temperature and mean velocity, which can be inferred from the results in figure 7(*b*).

4.2. *Fluctuating thermodynamic statistics*

Figure 9 shows the variation of thermodynamic fluctuations along the wall-normal distance, such as $\rho'_{rms}/\bar{\rho}$ in the inner scaling, $T'_{rms}/\bar{T}$ in the inner scaling, and p'_{rms}/τ_w in the inner scaling and outer scaling, respectively. As the Mach number increases, the peak of r.m.s. density fluctuations ρ'_{rms} and r.m.s. temperature fluctuations T'_{rms} at the boundary layer edge increases, and as the wall temperature decreases, a secondary peak of temperature fluctuations occurs in the buffer region due to the presence of a maximum value of the mean temperature $\bar{T}$ in the near-wall region at low wall temperatures, which enhances the contribution of the coupling of wall-normal velocity fluctuations v''_{rms} and mean temperature $\bar{T}$ to the r.m.s. temperature fluctuations, in agreement with the observations of Cogo *et al.* (2022). In the hypersonic turbulent boundary layer, the intensity of the r.m.s. pressure fluctuations p'_{rms} is enhanced as the Mach number increases and wall temperature decreases, which is consistent with the findings of Zhang *et al.* (2022) and Xu, Wang & Chen (2023). The bulk viscosity decreases the r.m.s. density fluctuations ρ'_{rms}, r.m.s. temperature fluctuations T'_{rms} and r.m.s. pressure fluctuations p'_{rms} in the inner layer of the boundary layer, especially in the viscous sublayer, where the reduction of thermodynamic fluctuations is more significant. This is because the rapid change of the thermodynamic state of the gas in the near-wall region of the boundary layer causes a non-equilibrium between the thermodynamic and mechanical pressures, and the bulk viscosity rebalances the two pressures by reducing the fluctuations of the thermodynamic quantities of the fluid in the boundary layer. As the Mach number increases or the wall temperature decreases, the effect of bulk viscosity becomes more significant.

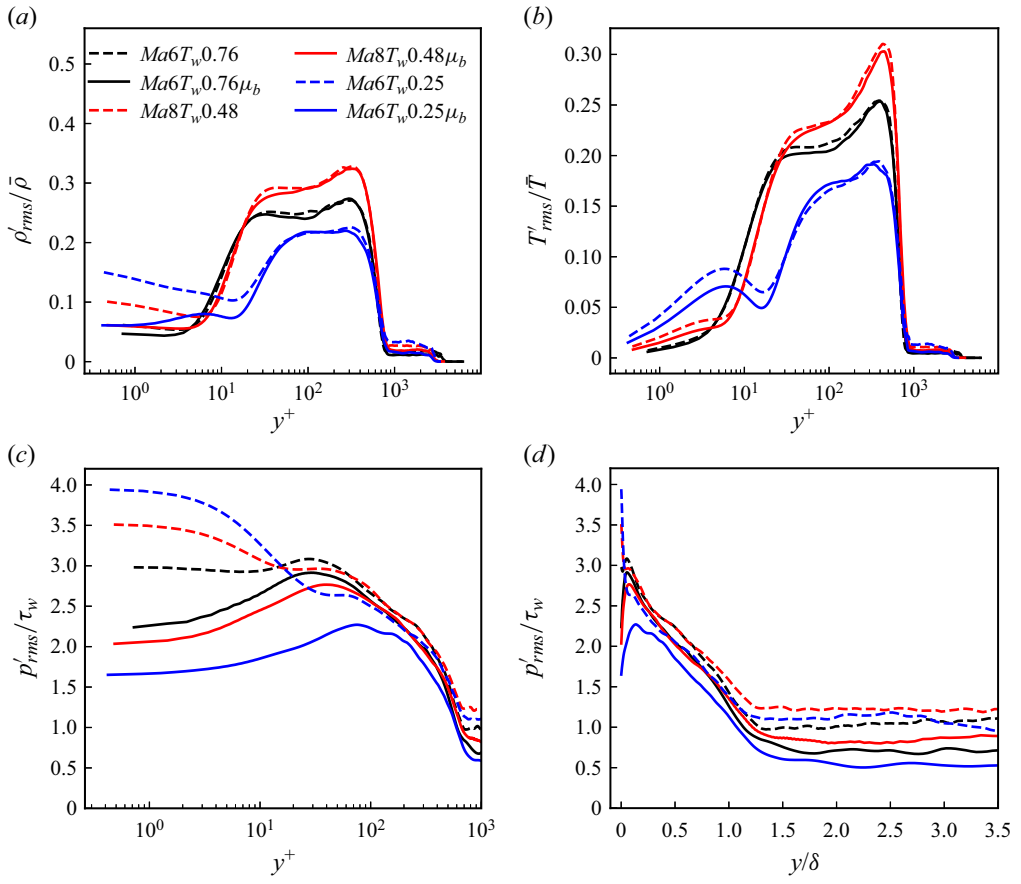

Figure 9. Profiles of the r.m.s. thermodynamic fluctuations for different cases along the wall-normal distance: (*a*) the r.m.s. density fluctuations scaled by mean density $\rho'_{rms}/\bar{\rho}$ in the inner scaling y^+; (*b*) the r.m.s. temperature fluctuations scaled by mean temperature $T'_{rms}/\bar{T}$ in the inner scaling y^+; and the r.m.s. pressure fluctuations scaled by wall shear stress p'_{rms}/τ_w in (*c*) the inner scaling y^+ and (*d*) the outer scaling y/δ.

4.3. *The strong Reynolds analogy*

Next, the impact of bulk viscosity on the relation between velocity fluctuations and temperature fluctuations is investigated. The turbulent Prandtl number and the correlation of velocity fluctuations and temperature fluctuations (Morkovin 1962) are

$$Pr_t = \frac{\overline{\rho u'' v''}\,\partial\tilde{T}/\partial y}{\overline{\rho v'' T''}\,\partial\tilde{u}/\partial y} \approx 1, \tag{4.3}$$

$$R_{u''T''} = \frac{\widetilde{uT} - \tilde{u}\tilde{T}}{u''_{rms}T''_{rms}}. \tag{4.4}$$

As shown in figure 10(*a*), the effect of bulk viscosity on the turbulent Prandtl number Pr_t can be neglected. The turbulent Prandtl number Pr_t is approximately 1 in the whole boundary layer, indicating that the turbulent Prandtl number is not affected by the variation of Mach number, wall temperature and other conditions. As shown in figure 10(*b*), $-R_{u''T''}$ remains at approximately 0.6 over most of the boundary layer, in agreement with the results obtained by Guarini *et al.* (2000) and Huang *et al.* (2022). Since the mean temperature

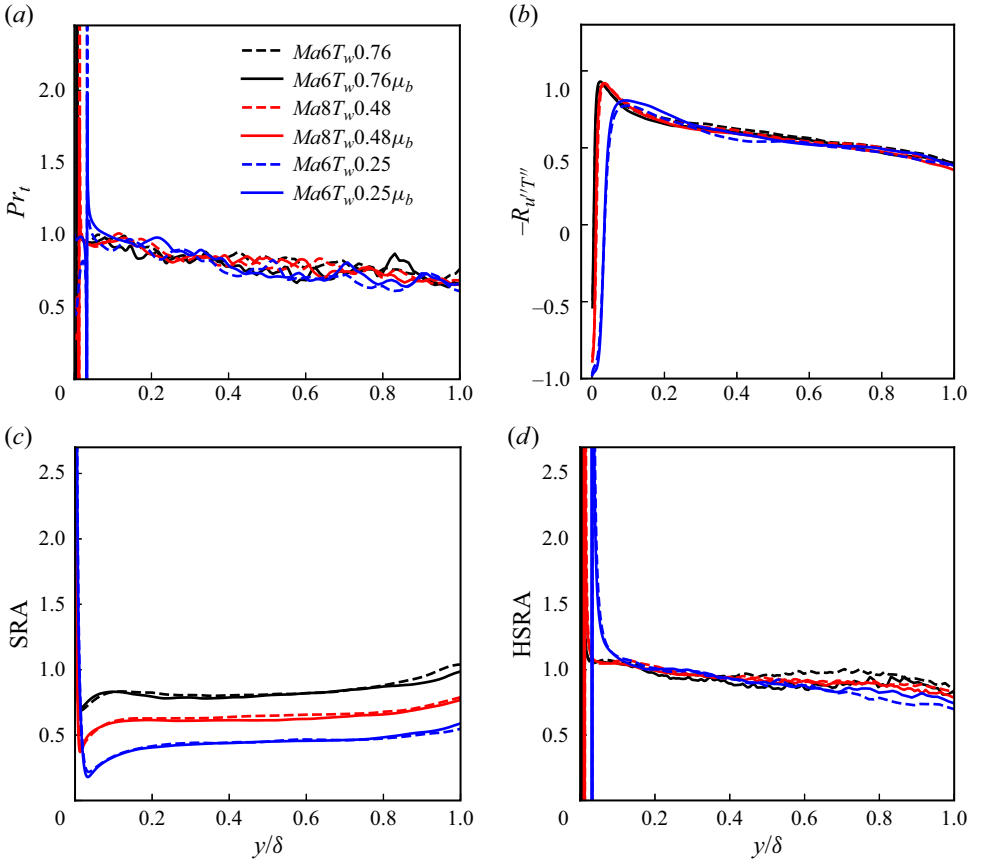

Figure 10. Relation between temperature fluctuations and velocity fluctuations: (*a*) turbulent Prandtl number Pr_t; (*b*) temperature–velocity correlation coefficient $-R_{u''T''}$; (*c*) the SRA relations; and (*d*) the modified SRA proposed by Huang (HSRA).

maximum will shift to the right when the wall temperature decreases, as shown in figure 7(*c*), $-R_{u''T''}$ will shift to the right, which is consistent with Coleman, Kim & Moser (1995), Duan *et al.* (2010) and Huang *et al.* (2022). Notably, the mean and fluctuating streamwise velocity and temperature are almost unaffected by the bulk viscosity in the log region and the outer layer. Therefore, the bulk viscosity has little effect on the correlation between velocity fluctuations and temperature fluctuations within most of the boundary layers.

Figure 10(*c*) shows the strong Reynolds analogy (SRA) theory for different cases. The SRA theory was proposed by Morkovin (1962) for analysing the correlation between temperature fluctuations and velocity fluctuations as follows:

$$\frac{T''_{rms}/\tilde{T}}{(\gamma-1)\,Ma^2\,(u''_{rms}/\tilde{u})} \approx 1. \tag{4.5}$$

By considering the variation of wall heat flux and eliminating wall temperature dependence, Gaviglio (1987), Rubesin (1990) and Huang *et al.* (1995) proposed a modified

SRA (GSRA, RSRA, HSRA, respectively) of the form

$$\frac{T''_{rms}/\tilde{T}}{(\gamma-1)\,Ma^2\,(u''_{rms}/\tilde{u})} \approx \frac{1}{c(1-\partial\widetilde{T}_t/\partial\widetilde{T})}, \tag{4.6}$$

where c is 1.0, 1.34 and Pr_t, respectively. It can be found from figure 10(c) that the effect of bulk viscosity on the SRA theory can be neglected. Looking at the left-hand side of the above equation, it can be seen that it is a function of temperature and velocity fluctuations. From the previous results, it can be seen that the temperature fluctuations and velocity fluctuations are affected by the wall temperature, therefore, when the wall temperature changes, the SRA theory is no longer applicable, which is consistent with the results of Martin (2007) and Duan *et al.* (2011). As shown in figure 10(d), by considering the effect of the wall heat flux, the generalized Reynolds analogy theory modified by Huang *et al.* (1995) (HSRA) is able to well describe the relation between temperature fluctuations and velocity fluctuations for wall-cooling cases, so that the HSRA of the cases under different working conditions is close to 1. Additionally, bulk viscosity has almost no effect on the HSRA, and this result is not affected by the variations of Mach number and wall temperature.

4.4. *Heat flux distribution*

Figure 11 shows the distributions of the heat flux and skin friction coefficient. Figures 11(a,b) plot the distributions of the skin friction coefficient C_f and wall conductive heat flux $-k\,\partial T/\partial y$ with the relative streamwise distance x/L_x, respectively. In order to make it easier to compare the statistics of different cases in the same figure, the streamwise location x is normalized by the streamwise length of computational domain L_x (Xu *et al.* 2022). As shown in the figures, the skin friction coefficient C_f and wall conductive heat flux $-k\,\partial T/\partial y$ will not vary with the streamwise distance when the turbulent boundary layer is sufficiently evolved. And the skin friction coefficient C_f increases as the wall temperature decreases, which is consistent with the conclusion of Zhang *et al.* (2022). However, after considering bulk viscosity, the skin friction coefficient C_f decreases slightly as the wall temperature decreases. As the Mach number increases and the wall temperature decreases, the wall conductive heat flux $-k\,\partial T/\partial y$ increases. If the influence of thermal conductivity coefficient k is not considered temporarily, then it indicates that the wall-normal temperature gradient $\partial T/\partial y$ increases. This conclusion is consistent with what we obtained in § 4.1. In addition, the effect of bulk viscosity on wall conductive heat flux $-k\partial T/\partial y$ is negligible. Figures 11(c,d) plot the variation of the conductive heat flux $-k\,\partial T/\partial y$ and turbulent heat flux $\overline{\rho v''T''}$ with the wall-normal distance in inner scaling y^+, respectively. From the figures, it can be seen that the conductive heat flux $-k\,\partial T/\partial y$ is dominant, and the turbulent heat flux $\overline{\rho v''T''}$ is very small in the near-wall region due to the velocity in the viscous sublayer being approximately 0. The total heat flux inside the viscous sublayer is determined mainly by the conductive heat flux $-k\,\partial T/\partial y$. In the log region, both the wall-normal velocity fluctuations v'' and the temperature fluctuations T'' reach their maximum values, while the mean temperature gradient $\partial T/\partial y$ decreases as the wall distance increases, so that the total heat flux magnitude in the log region depends mainly on the turbulent heat flux $\overline{\rho v''T''}$. Due to the effect of dilatational dissipation, the bulk viscosity weakens the compressibility of the hypersonic turbulent boundary layer, and the wall-normal velocity fluctuations and temperature fluctuations decrease in the viscous sublayer, so the turbulent heat flux $\overline{\rho v''T''}$ decreases slightly in both the viscous

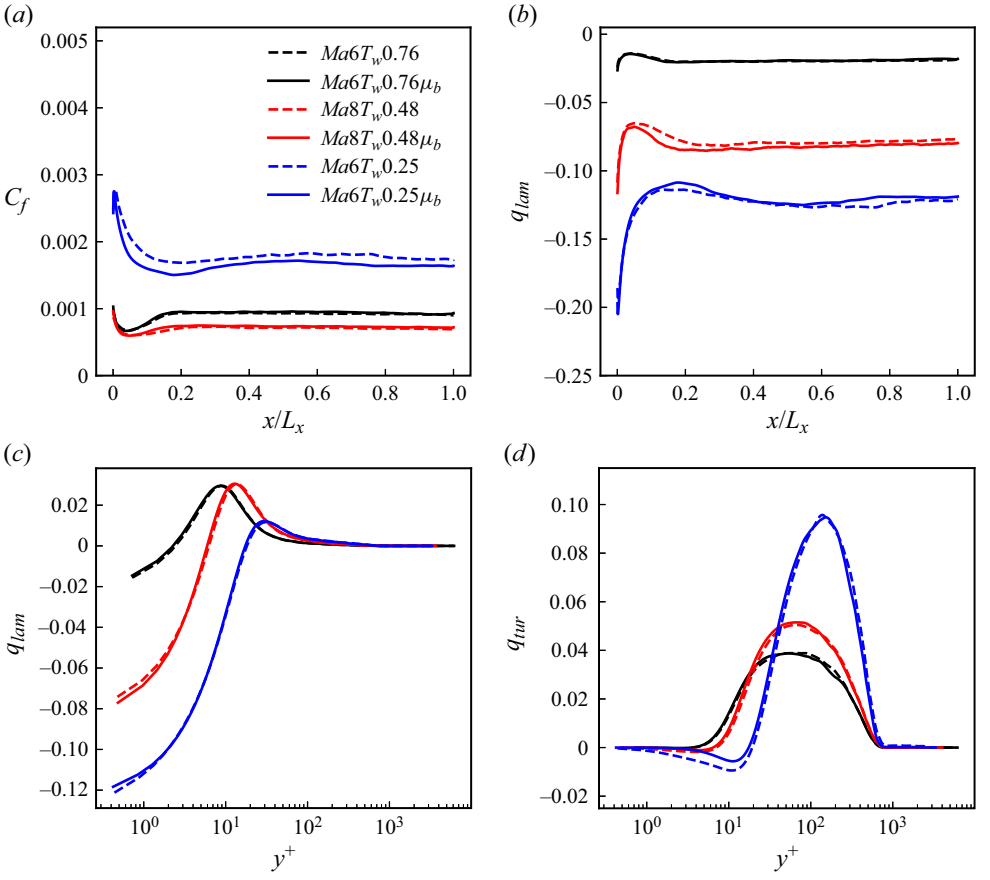

Figure 11. Heat flux and skin friction coefficient. The distributions of (*a*) the skin friction coefficient C_f and (*b*) the conductive heat flux $-k\partial T/\partial y$ with the relative streamwise coordinates x/L_x, where L_x is the length of the computational domain in the streamwise direction. The wall-normal distributions of (*c*) the conductive heat flux $-k\,\partial T/\partial y$ and (*d*) the wall-normal turbulent heat flux $\overline{\rho v'' T''}$.

sublayer and the log layer of the boundary layer by considering bulk viscosity. In contrast, bulk viscosity has almost no effect on the mean temperature, so bulk viscosity has less effect on the thermal conductivity heat flux $-k\,\partial T/\partial y$, and in conclusion, bulk viscosity decreases slightly the total heat flux in the viscous sublayer and log layers. In addition, the wall-normal turbulent heat flux $\overline{\rho v'' T''}$ increases significantly with increasing Mach number, which is consistent with the results of Huang *et al.* (2020, 2022).

5. Turbulent structures

In order to reveal further the effect of bulk viscosity on hypersonic boundary layer flow, the turbulent structures are analysed in this section. Figure 12 reports the instantaneous vortical structures of the hypersonic turbulent boundary layer based on the Q-criterion (Hunt, Wray & Moin 1988). The large-scale vortex structures in the outer layer become richer when the Mach number increases (figures 12*a*,*c*), while the spanwise spacing of the large-scale vortex structures becomes larger as the wall temperature decreases (figures 12*a*,*e*), which is consistent with the conclusion of Huang *et al.* (2022).

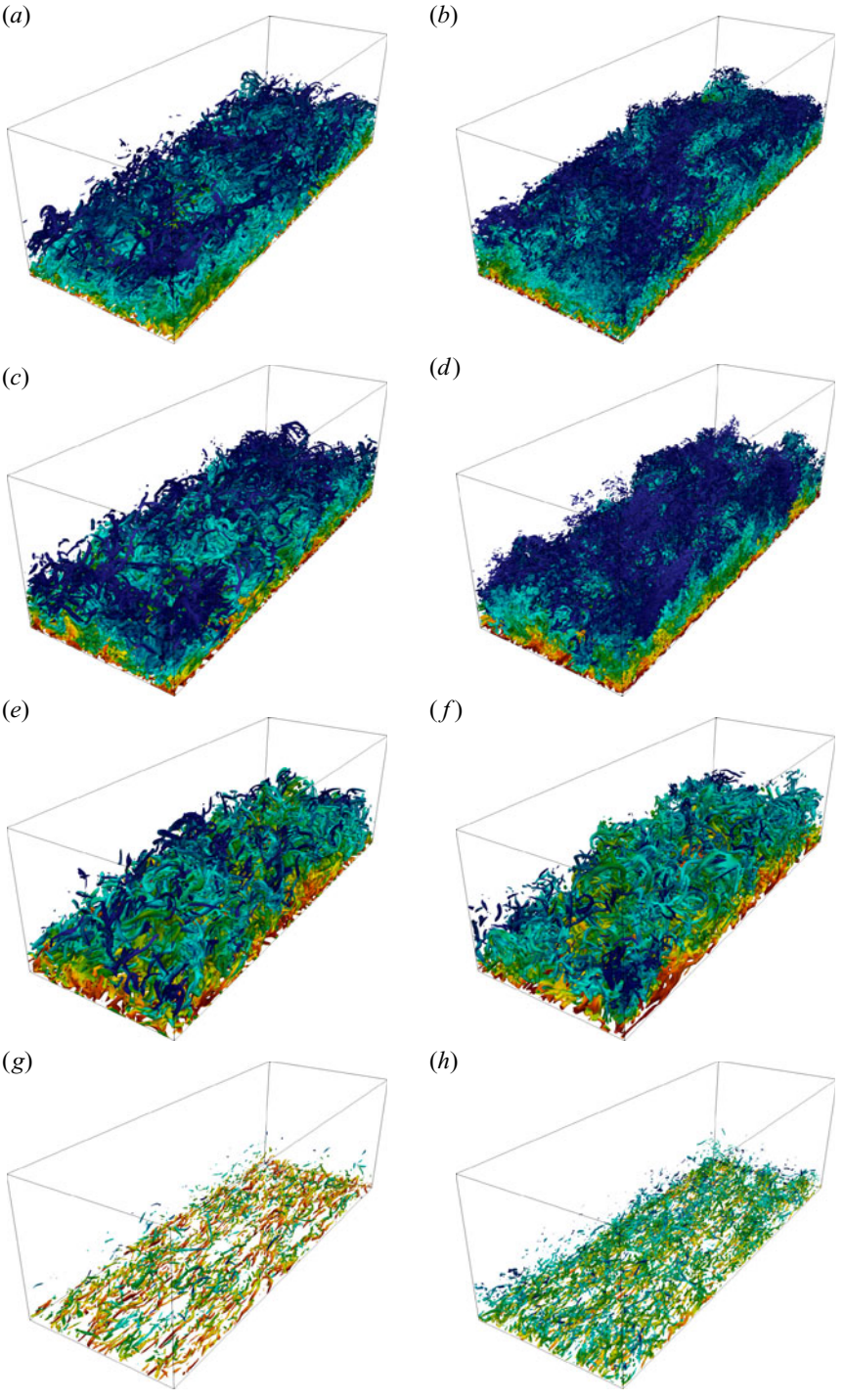

Figure 12. Snapshots of instantaneous vortical structures based on the Q-criterion for (*a*,*b*) $Ma6T_w0.76$, (*c*,*d*) $Ma8T_w0.48$ and (*e*,*f*) $Ma6T_w0.25$ for $Q = 20$, and (*g*,*h*) $Ma6T_w0.76$ for $Q = 300$ – (*b*,*d*,*f*,*h*) with and (*a*,*c*,*e*,*g*) without bulk viscosity. The colour of the vortex structure changes from red to blue along the wall-normal directions. The size of the box is $\Delta x \times \Delta y \times \Delta z = 8\delta_i \times 3\delta_i \times 3\delta_i$.

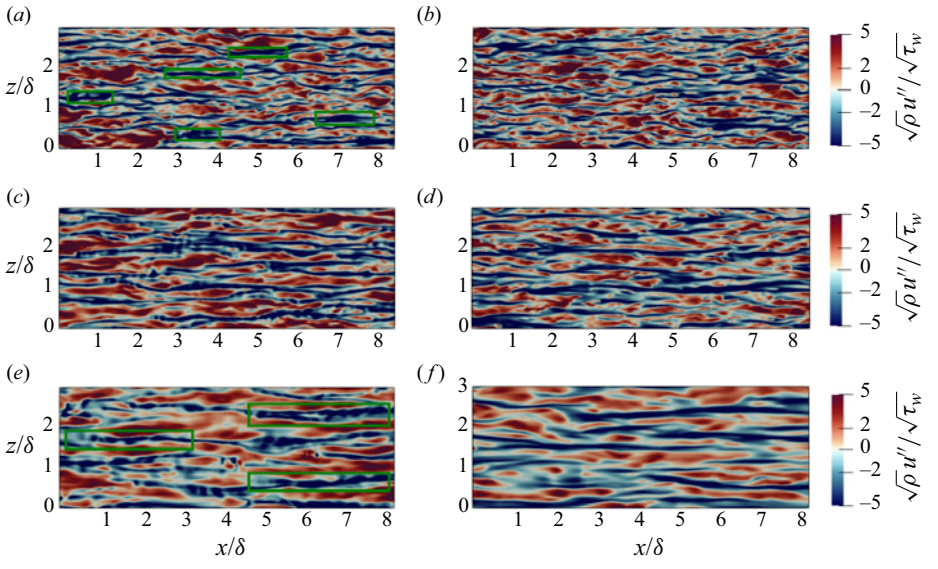

Figure 13. Instantaneous streamwise velocity fluctuations u'' normalized by the friction velocity $u_\tau^* = \sqrt{\tau_w/\rho}$ in a wall-parallel slice at $y^+ = 15$ for different cases: (*a*) $Ma6T_w0.76$, (*b*) $Ma6T_w0.76\mu_b$, (*c*) $Ma8T_w0.48$, (*d*) $Ma8T_w0.48\mu_b$, (*e*) $Ma6T_w0.25$, (*f*) $Ma6T_w0.25\mu_b$ – (*a*,*c*,*e*) without bulk viscosity ($\mu_b/\mu = 0$), and (*b*,*d*,*f*) with bulk viscosity ($\mu_b/\mu = 100$).

When considering bulk viscosity, the large-scale vortex structure within the boundary layer becomes fragmented, and the small-scale vortex structure becomes richer by comparing figures 12(*g*,*h*).

Figure 13 displays the instantaneous fields of normalized streamwise velocity fluctuations $\sqrt{\rho}\,u''/\sqrt{\tau_w}$ in a wall-parallel slice at $y^+ = 15$ at the selected stations. The alternating distribution of high and low velocity momentum forms the velocity striping structure in this figure, which is related to the ejection and sweep events. Those structures have been observed widely in both incompressible (Jiménez 2013) and compressible (Bernardini & Pirozzoli 2011; Bross, Scharnowski & Khler 2021; Xu *et al.* 2022) turbulence. Those large-scale coherent structures can reach several boundary layer thicknesses in the streamwise direction, and contain a large part of the turbulent kinetic energy (Bross *et al.* 2021). The near-wall streaks are similar for different Mach numbers, such as figures 13(*a*,*c*), which is consistent with the findings of Duan *et al.* (2011). As shown in figures 13(*a*) and 13(*e*), the near-wall streaks marked by the rectangular boxes become thicker and more coherent as the wall temperature decreases, in agreement with the observation of Duan *et al.* (2010), Lagha *et al.* (2011), Huang *et al.* (2022) and Zhang *et al.* (2022). The effect of bulk viscosity on the instantaneous fields of streamwise fluctuating velocity $\sqrt{\rho u''}/\sqrt{\tau_w}$ is negligible.

Figures 14 and 15 present the instantaneous fields of normalized density fluctuations $\rho'/\bar{\rho}$ and normalized temperature fluctuations $T'/\bar{T}$ in a wall-parallel slice at $y^+ = 15$, respectively. It can be observed from the figures that the instantaneous fields of normalized density fluctuations $\rho'/\bar{\rho}$ and normalized temperature fluctuations $T'/\bar{T}$ exhibit travelling-wave-like alternating positive and negative structures (TAPNS), which is similar to the fluctuating velocity streaks (Xu *et al.* 2023). In addition, the similar near-wall streak structures of the fluctuating temperature and fluctuating velocity instantaneous fields can be corroborated with the temperature and velocity fluctuations correlation

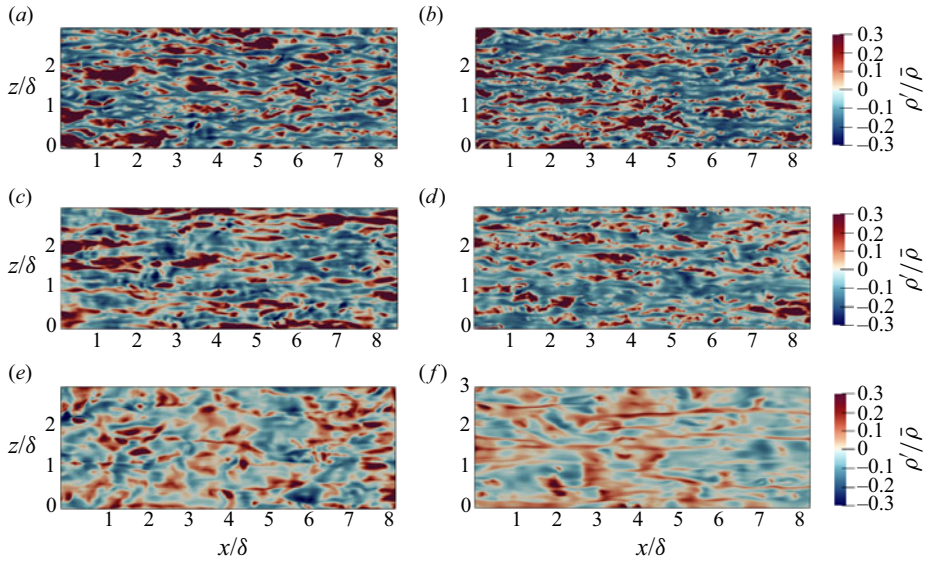

Figure 14. Instantaneous density fluctuations ρ' normalized by the mean density $\bar{\rho}$ in a wall-parallel slice at $y^+ = 15$ for different cases: (*a*) $Ma6T_w0.76$, (*b*) $Ma6T_w0.76\mu_b$, (*c*) $Ma8T_w0.48$, (*d*) $Ma8T_w0.48\mu_b$, (*e*) $Ma6T_w0.25$, (*f*) $Ma6T_w0.25\mu_b$ – (*a*,*c*,*e*) without bulk viscosity ($\mu_b/\mu = 0$), and (*b*,*d*,*f*) with bulk viscosity ($\mu_b/\mu = 100$).

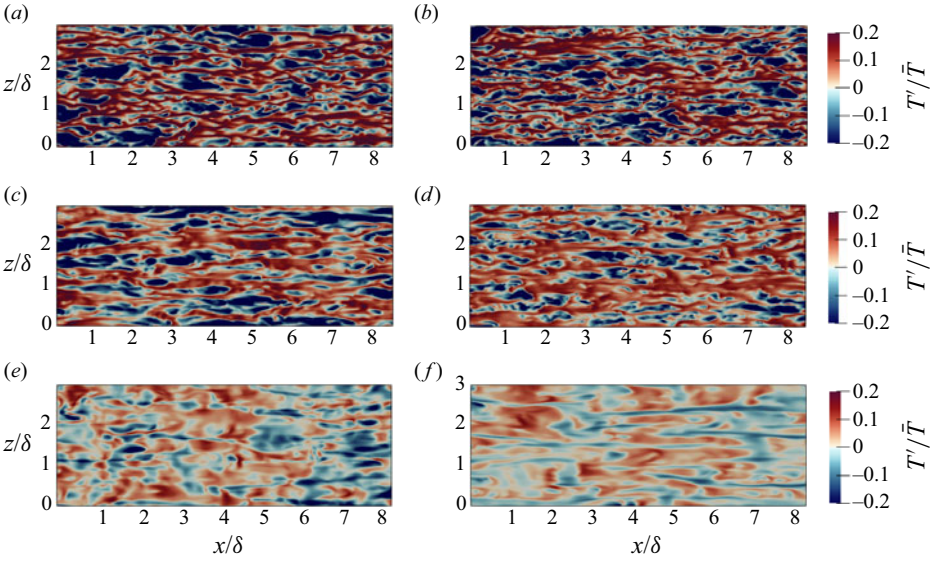

Figure 15. Instantaneous temperature fluctuations T' normalized by the mean temperature $\bar{T}$ in a wall-parallel slice at $y^+ = 15$ for different cases: (*a*) $Ma6T_w0.76$, (*b*) $Ma6T_w0.76\mu_b$, (*c*) $Ma8T_w0.48$, (*d*) $Ma8T_w0.48\mu_b$, (*e*) $Ma6T_w0.25$, (*f*) $Ma6T_w0.25\mu_b$ – (*a*,*c*,*e*) without bulk viscosity ($\mu_b/\mu = 0$), and (*b*,*d*,*f*) with bulk viscosity ($\mu_b/\mu = 100$).

approximating to 1, which was also reported by Xu *et al.* (2021*a*, 2022) and Cogo *et al.* (2022). Moreover, comparing the figures with and without bulk viscosity, the density fluctuations $\rho'/\bar{\rho}$ and temperature fluctuations $T'/\bar{T}$ in the near-wall region decrease

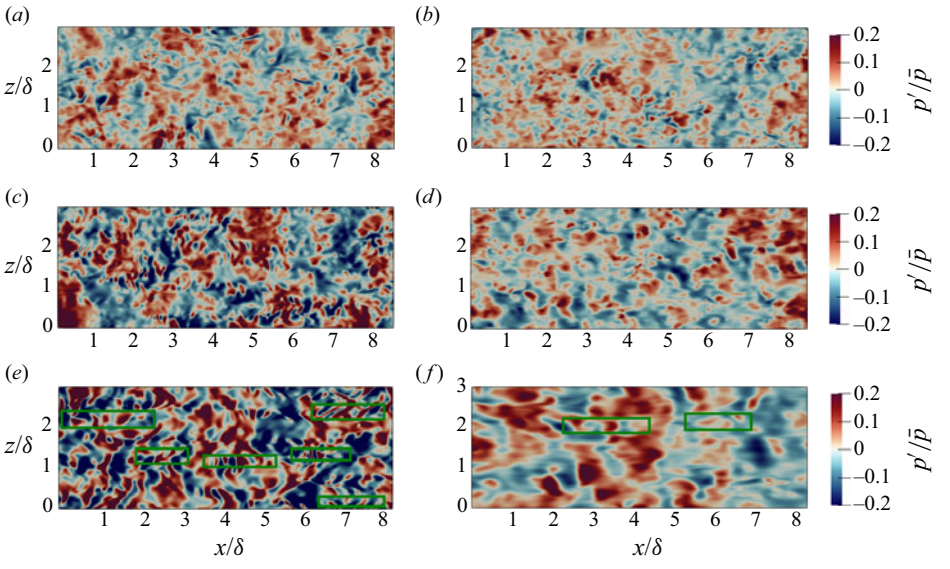

Figure 16. Instantaneous pressure fluctuations p' normalized by the mean pressure $\bar{p}$ in a wall-parallel slice at $y^+ = 5$ for different cases: (*a*) $Ma6T_w0.76$, (*b*) $Ma6T_w0.76\mu_b$, (*c*) $Ma8T_w0.48$, (*d*) $Ma8T_w0.48\mu_b$, (*e*) $Ma6T_w0.25$, (*f*) $Ma6T_w0.25\mu_b$ – (*a*,*c*,*e*) without bulk viscosity ($\mu_b/\mu = 0$), and (*b*,*d*,*f*) with bulk viscosity ($\mu_b/\mu = 100$).

slightly after considering the bulk viscosity, which is consistent with the results in figure 9. Additionally, the effect of bulk viscosity on TAPNS of normalized density and temperature fluctuations is negligible in the compressible turbulent boundary layer.

Figure 16 shows the instantaneous fields of normalized pressure fluctuations $p'/\bar{p}$ in a wall-parallel slice at $y^+ = 5$. It can be observed from the figure that the instantaneous fields of normalized pressure fluctuations $p'/\bar{p}$ present the TAPNS, which were also reported by Zhang *et al.* (2022) and Xu *et al.* (2023). As shown in figures 16(*a*) and 16(*e*), the intensity of pressure fluctuations $p'/\bar{p}$ and the TAPNS are increased as the wall temperature decreases, indicating that wall cooling enhances the compressibility of the fluid in the near-wall region, which is consistent with the conclusion of Zhang *et al.* (2022) and Xu *et al.* (2023). Moreover, comparing the figures with and without bulk viscosity, the intensity of pressure fluctuations $p'/\bar{p}$ and the TAPNS marked by the rectangular boxes in the near-wall region decrease distinctly after considering the bulk viscosity, indicating that the bulk viscosity reduces the compressibility of fluid in the near-wall region.

6. Small-scale properties

The role of bulk viscosity on small-scale properties is studied in this section. Figures 17 and 18 plot the probability density function (PDF) of the normalized derivative of the streamwise velocity fluctuations u' with respect to streamwise coordinate x and wall-normal coordinate y in the different part of turbulent boundary layer, respectively. As can be seen from figure 17, for the absolute value of the fluctuating velocity derivative with respect to streamwise coordinate $|\partial u'/\partial x|$ greater than 5 in the viscous sublayer, the PDF of fluctuating velocity derivative $\partial u'/\partial x$ of the compressible turbulent boundary layer is significantly larger than that of the compressible homogeneous isotropic turbulence (HIT) and homogeneous shear turbulence (HST), which indicates qualitatively that the

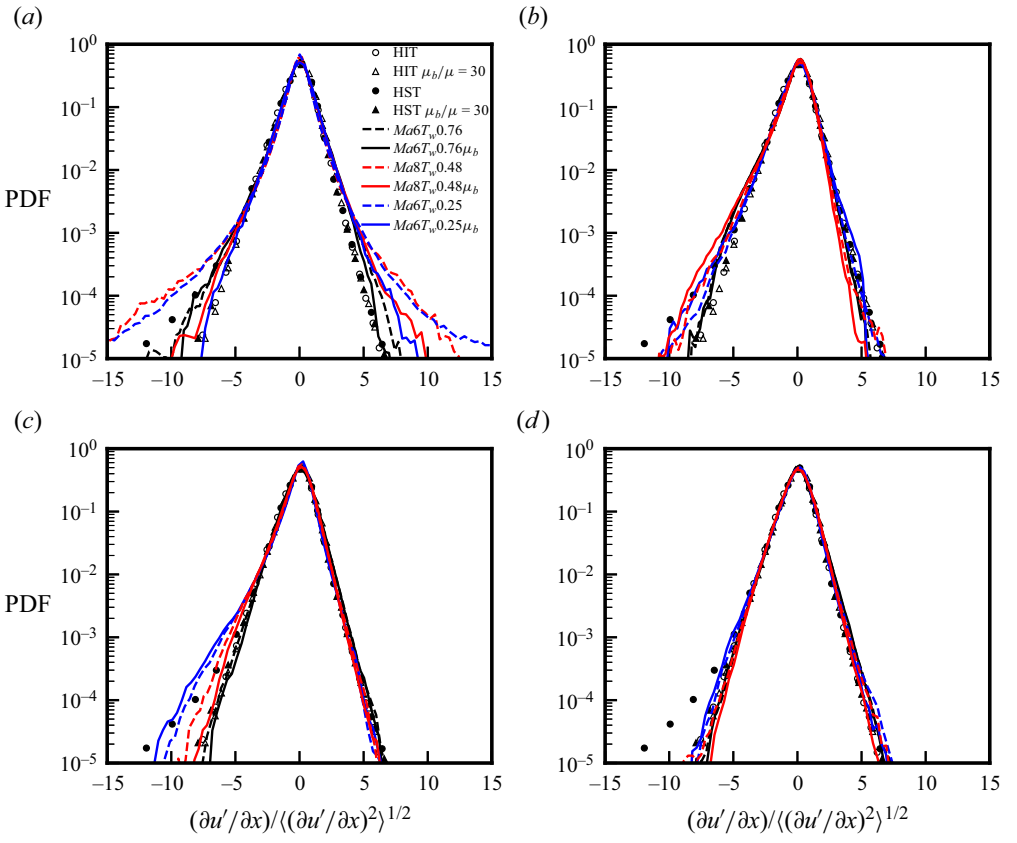

Figure 17. The PDF of the normalized derivative of the streamwise velocity fluctuations u' with respect to streamwise coordinate x in the different parts of the turbulent boundary layer: (*a*) viscous sublayer, (*b*) buffer layer, (*c*) log layer, and (*d*) outer layer. Symbols from Chen *et al.* (2019): ◯, HIT without bulk viscosity; △, HIT with bulk-to-shear viscosity ratio 30; ●, HST without bulk viscosity; ▲, HST with bulk-to-shear viscosity ratio 30.

fluctuation intensity of the viscous sublayer of the compressible turbulent boundary layer is stronger than that of HIT and HST. Meanwhile, in the inner layer of the boundary layer, the probability density distribution of the fluctuating velocity derivative is more similar to that of HST, indicating a stronger shear effect in the compressible turbulent boundary layer. As the wall-normal distance increases, the probability density distribution of the fluctuating velocity derivative in the outer layer of the boundary layer approaches that of HIT, indicating that the outer layer of the boundary layer is nearly isotropic. The bulk viscosity decreases the fluctuating velocity derivative $\partial u'/\partial x$ within the viscous sublayer of the compressible turbulent boundary layer, and the PDF for the absolute value of the fluctuating velocity derivative greater than 5 decreases, while in the buffer, log and outer layers of the boundary layer, the effect of bulk viscosity on the fluctuating velocity derivative can be neglected. As can be seen in figure 18, the maximum negative values of the fluctuating velocity derivative with respect to wall-normal coordinate $\partial u'/\partial y$ in the viscous sublayer and buffer layer are smaller comparing with its maximum positive values due to the effect of the wall of the compressible turbulent boundary layer. In the log layer and outer layer of the boundary layer, the distribution of the PDF of the fluctuating velocity derivative with respect to wall-normal coordinate is similar to that of HIT and HST.

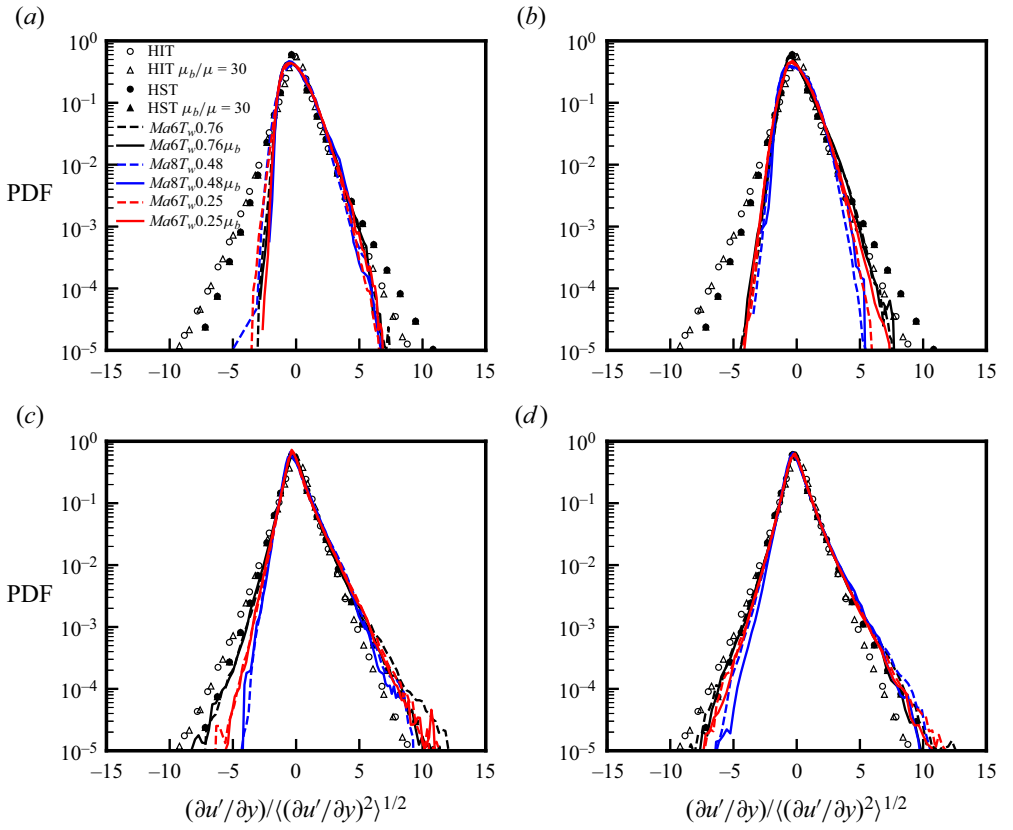

Figure 18. The PDF of the normalized derivative of the streamwise velocity fluctuations u' with respect to wall-normal coordinate y in the different parts of the turbulent boundary layer: (*a*) viscous sublayer, (*b*) buffer layer, (*c*) log layer, and (*d*) outer layer. Symbols from Chen *et al.* (2019): ◯, HIT without bulk viscosity; △, HIT with bulk-to-shear viscosity ratio 30; ●, HST without bulk viscosity; ▲, HST with bulk-to-shear viscosity ratio 30.

The effect of bulk viscosity on the fluctuating velocity derivative with respect to wall-normal coordinate $\partial u'/\partial y$ in the compressible turbulent boundary layer is negligible, which is consistent with the conclusions of Chen *et al.* (2019).

The PDF of the dilatation $\theta = \partial u/\partial x + \partial v/\partial y + \partial w/\partial z$ in four different parts of the turbulent boundary layer are shown in figure 19 to assess the compressibility of fluids. The compression ($\theta < 0$) and expansion ($\theta > 0$) of the fluids are enhanced significantly with increasing Mach number and increasing wall temperature by comparing the dashed lines in the figure, as reported by Lagha *et al.* (2011). However, the compression and expansion effects of the fluids gradually diminish with increasing wall-normal distance. The compression of the fluids is weakened significantly in the turbulent boundary layer when bulk viscosity is considered, which is consistent with the conclusions of Pan & Johnsen (2017) and Chen *et al.* (2019).

The shear stress budget in the near-wall region of the turbulent boundary layer is of great significance for turbulence modelling and understanding the interaction of small-scale structures in the inner layer. Meanwhile, the total stress is approximately equal to the sum of the viscous shear stress and Reynolds shear stress in the near-wall region, which is the physical basis for the modelling of the mean velocity transformations of the viscous

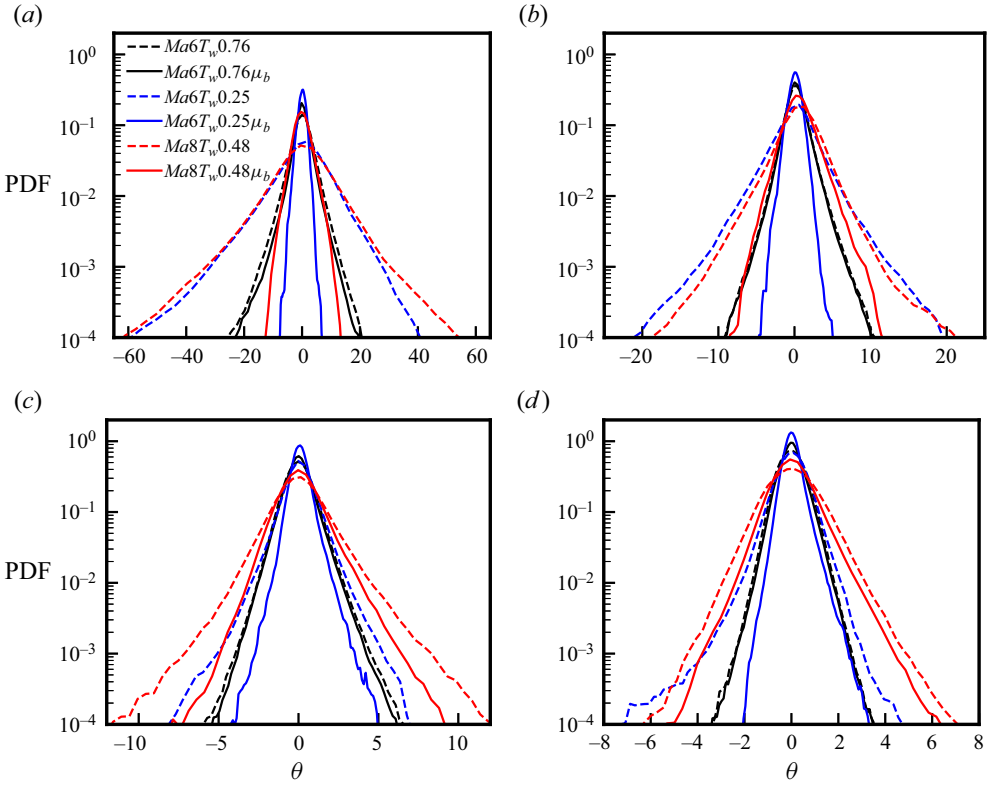

Figure 19. The PDF of the dilatation θ for different cases in different parts of the turbulent boundary layer: (*a*) viscous sublayer, (*b*) buffer layer, (*c*) log layer and (*d*) outer layer.

sublayer and the buffer layer. Recently, Lee *et al.* (2023) conducted a detailed analysis of the effects of density and viscosity fluctuations on the viscous, Reynolds and total shear stresses in the near-wall region, and found that the sum of generalized viscous shear stress and Reynolds shear stress can better approximate 1 in the viscous sublayer. The equation of the generalized shear stress budget in the near-wall region of turbulent boundary layer is

$$1 = \left[\frac{\bar{\mu}}{\tau_w}\frac{\partial \tilde{u}}{\partial y} + \left(\frac{\overline{\bar{\mu}\,\partial u''}}{\partial y} + \overline{\mu'\frac{\partial u''}{\partial y}}\right)\Big/\tau_w\right] - \frac{\bar{\rho}\,\widetilde{u''v''}}{\tau_w} = [\tau_V^+ + \zeta_\mu^+] + \tau_R^+, \tag{6.1}$$

where τ_V^+ is the Favre-averaged viscous shear stress, ζ_μ^+ is the influence arising from viscosity fluctuations, the sum of τ_V^+ and ζ_μ^+ is defined as the generalized viscous shear stress τ_{VG}^+, and τ_R^+ is the Favre-averaged Reynolds shear stress.

Figure 20 shows the wall-normal distributions of the generalized shear stress budget in the semi-local scaling. As shown in figure 20(*a*), due to the consideration of bulk viscosity, the viscosity fluctuations in the near-wall region are enhanced, so that the fluctuating viscosity term ζ_μ^+ increases in the viscous sublayer. And the generalized viscous shear stress τ_{VG}^+ also increases slightly in the viscous sublayer, as shown in figure 20(*b*). The Reynolds shear stress shown in figure 20(*c*) is the same as that in figure 4(*b*).

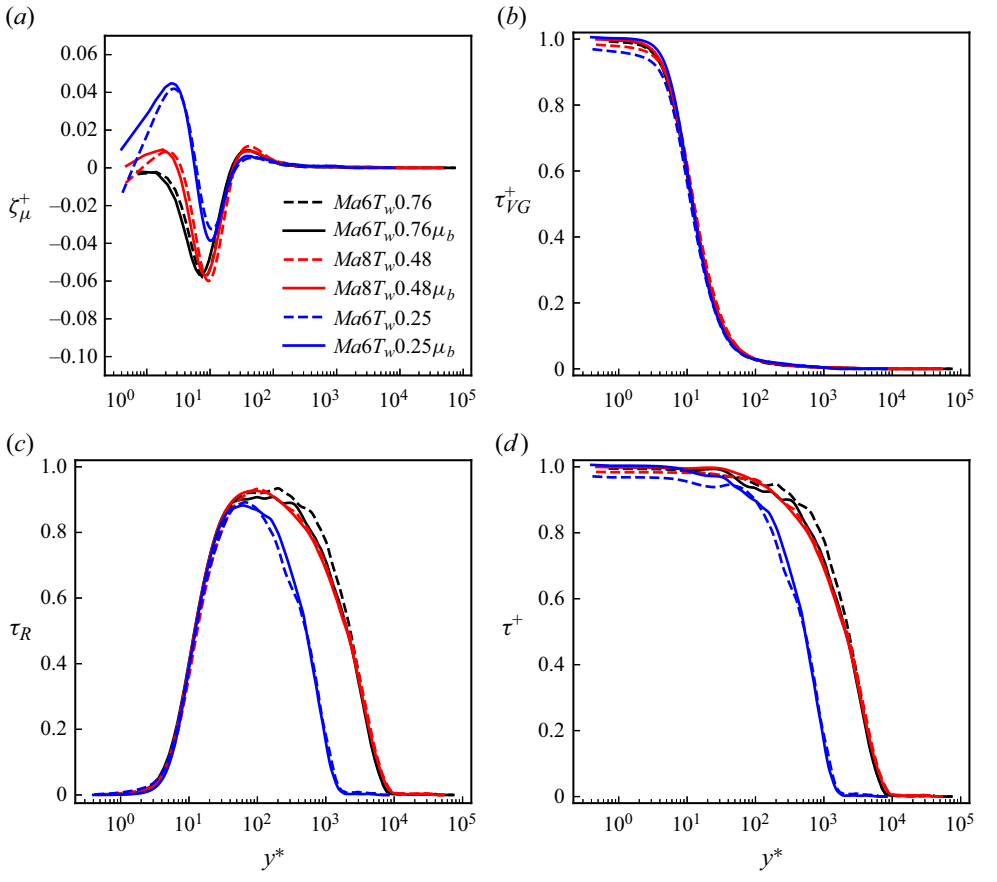

Figure 20. The shear stress budget in the compressible turbulent boundary layer for different cases: (*a*) viscosity fluctuation term ζ_μ^+, (*b*) generalized viscous shear stress $\tau_{VG}^+ = \tau_V^+ + \zeta_\mu^+$, (*c*) Reynolds shear stress τ_R^+ and (*d*) total stress τ^+ along the wall-normal distance in the semi-local scaling.

After considering the bulk viscosity, the compressibility of turbulent boundary layer decreases, so the peak of Reynolds shear stress τ_R^+ is reduced slightly in the log layer. Figure 20(*d*) represents the generalized total stress budget taking into account the effect of density and viscosity fluctuations. Combining the effect of bulk viscosity on the generalized viscous and Reynolds shear stresses, it can be found that the generalized total stress τ^+ increases slightly in the viscous sublayer by considering the bulk viscosity, but the effect of the bulk viscosity on the total stress budget is kept in a negligible range, which is why the mean velocity transformation is still valid after considering the bulk viscosity.

7. Discussion of results

Throughout the entire paper, the influence of bulk viscosity on compressible turbulent boundary layers is characterized mainly by a notable decrease in wall-normal velocity fluctuations, thermodynamic fluctuations, and related quantities such as the pressure dilatation and pressure diffusion terms in the turbulent kinetic energy budget. This implies a substantial reduction in the compressibility of the turbulent boundary layer due to the presence of bulk viscosity. Subsequently, we try to analyse the physical mechanism

of how bulk viscosity induces a reduction in the wall-normal velocity fluctuations and thermodynamic fluctuations in the near-wall region of turbulent boundary layer.

In order to reveal the physical mechanism of the effect of bulk viscosity on the wall-normal velocity fluctuations, this paper further investigates the wall-normal Reynolds stress budgets in compressible turbulent boundary layers. The Favre-averaged Reynolds stress tensor is defined as $\tau_{ij} = \overline{\rho u_i'' u_j''}/\bar{\rho}$, and its transport equation is

$$\frac{\partial(\bar{\rho}\tau_{ij})}{\partial t} + \frac{\partial(\bar{\rho}\tau_{ij}\widetilde{u_k})}{\partial x_k} = P_{ij} + T_{ij} + \Pi_{ij} - \bar{\rho}\epsilon_{ij} + D_{ij} + M_{ij}, \tag{7.1}$$

where

$$P_{ij} = -\left(\overline{\rho u_i'' u_k''}\frac{\partial \widetilde{u_j}}{\partial x_k} + \overline{\rho u_j'' u_k''}\frac{\partial \widetilde{u_i}}{\partial x_k}\right), \tag{7.2a}$$

$$T_{ij} = -\frac{\partial}{\partial x_k}(\overline{\rho u_i'' u_j'' u_k''}), \tag{7.2b}$$

$$\Pi_{ij} = -\left(\overline{u_i''\frac{\partial p'}{\partial x_j}} + \overline{u_j''\frac{\partial p'}{\partial x_i}}\right), \tag{7.2c}$$

$$\bar{\rho}\epsilon_{ij} = \overline{\sigma_{ik}'\frac{\partial u_j''}{\partial x_k}} + \overline{\sigma_{jk}'\frac{\partial u_i''}{\partial x_k}}, \tag{7.2d}$$

$$D_{ij} = \frac{\partial}{\partial x_k}(\overline{\sigma_{ik}' u_j'' + \sigma_{jk}' u_i''}), \tag{7.2e}$$

$$M_{ij} = \overline{u_i''}\left(\frac{\partial \overline{\sigma_{kj}}}{\partial x_k} - \frac{\partial \bar{p}}{\partial x_j}\right) + \overline{u_j''}\left(\frac{\partial \overline{\sigma_{ki}}}{\partial x_k} - \frac{\partial \bar{p}}{\partial x_i}\right). \tag{7.2f}$$

The transport terms of Reynolds stress include the production term P_{ij}, turbulent diffusion term T_{ij}, velocity pressure-gradient term Π_{ij}, viscous dissipation term $-\bar{\rho}\epsilon_{ij}$, viscous diffusion term D_{ij}, and mass flux contribution term M_{ij} (Mansour, Kim & Moin 1988).

Figure 21 shows the wall-normal Reynolds stress budgets $\tau_{yy} = \overline{\rho v'' v''}/\bar{\rho}$. It can be observed that the transport of wall-normal Reynolds stress τ_{yy} in the buffer layer and log layer is determined mainly by the turbulent diffusion term T_{yy}, velocity pressure-gradient term Π_{yy}, and viscous dissipation term $-\bar{\rho}\epsilon_{yy}$ in the turbulent boundary layer. However, the production term P_{yy}, viscous diffusion term D_{yy}, and mass flux contribution term M_{yy} have little effect on the wall-normal Reynolds stress budgets, which was also reported by Smits *et al.* (2021) and Nicholson *et al.* (2022). The influence of bulk viscosity on the transport terms of wall-normal Reynolds stress can be ignored, except for the viscous dissipation term $-\bar{\rho}\epsilon_{yy}$. The bulk viscosity enhances mainly the viscous dissipation term $-\bar{\rho}\epsilon_{yy}$, thereby reducing significantly the wall-normal velocity fluctuations v''_{rms} in the near-wall region.

In order to provide more physical explanations, we decompose the pressure fluctuations p^+_{rms} into four components. The equation of the pressure fluctuation is (Yu, Xu & Pirozzoli 2020)

$$\frac{\partial^2 p'}{\partial x_i\,\partial x_i} = \frac{\partial^2 \sigma_{ij}'}{\partial x_i\,\partial x_j} - \frac{\partial^2}{\partial x_i\,\partial x_j}(2\rho\tilde{u}_i u_j'' + \rho'\tilde{u}_i\tilde{u}_j) - \frac{\partial^2}{\partial x_i\,\partial x_j}(\rho u_i'' u_j'' - \overline{\rho u_i'' u_j''}) + \frac{\partial^2 \rho'}{\partial t^2}. \tag{7.3}$$

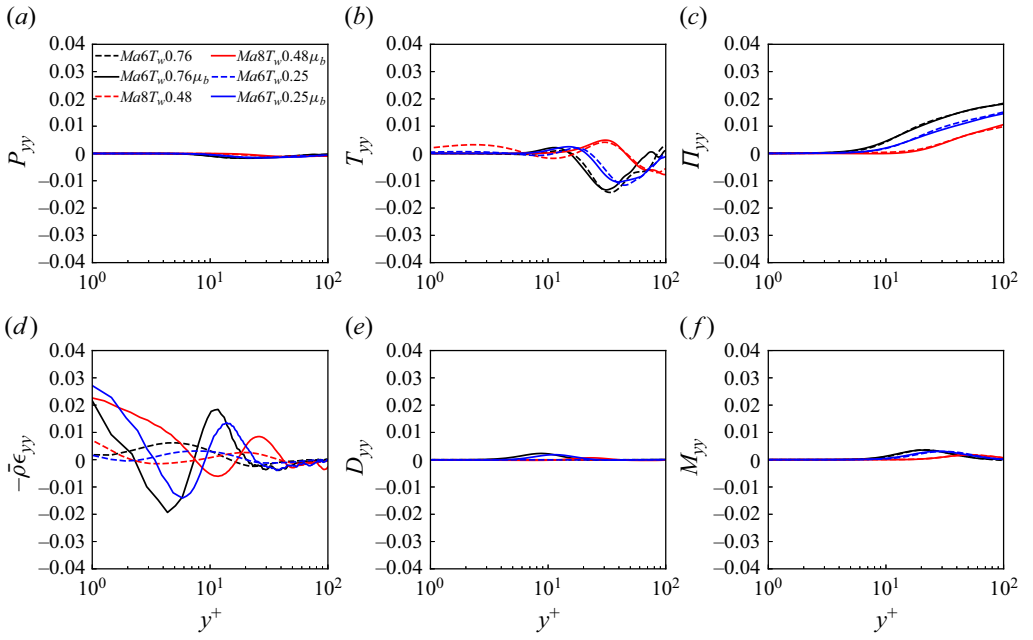

Figure 21. The wall-normal Reynolds stress budgets $\tau_{yy} = \overline{\rho v'' v''}/\bar{\rho}$. The wall-normal distributions of (*a*) production P_{yy}, (*b*) turbulent diffusion T_{yy}, (*c*) velocity pressure-gradient Π_{yy}, (*d*) viscous dissipation $-\bar{\rho}\epsilon_{yy}$, (*e*) viscous diffusion D_{yy} and (*f*) mass flux contribution M_{yy}, normalized by $\rho u_\tau^3/y_\tau$ in the inner scaling. Solid lines are for $\mu_b/\mu = 100$; dashed lines are for $\mu_b/\mu = 0$.

Based on the characterization of the right-hand-side terms of the pressure equation, the pressure is decomposed into (Tang *et al.* 2020)

$$p' = p_r + p_s + p_\sigma + p_c, \tag{7.4}$$

where p_r is the rapid pressure characterizing the linear mean shear–turbulence interactions, p_s is the slow pressure characterizing the nonlinear turbulence–turbulence interactions, p_σ represents the viscous pressure characterizing the contribution of viscous stresses to the pressure fluctuations, and p_c denotes the compressible pressure characterizing the contribution of the compressibility to the pressure fluctuations.

By comparing (7.3) and (7.4), the following four equations for fluctuating pressure components can be obtained, respectively:

$$\frac{\partial^2 p_r}{\partial x_i \partial x_i} = -2\frac{\partial \tilde{u}_i}{\partial x_j}\frac{\partial \rho u_j''}{\partial x_i}, \tag{7.5a}$$

$$\frac{\partial^2 p_s}{\partial x_i \partial x_i} = -\frac{\partial^2}{\partial x_i \partial x_j}(\rho u_i'' u_j'' - \overline{\rho u_i'' u_j''}), \tag{7.5b}$$

$$\frac{\partial^2 p_\sigma}{\partial x_i \partial x_i} = \frac{\partial^2 \sigma_{ij}'}{\partial x_i \partial x_j}, \tag{7.5c}$$

$$\frac{\partial^2 p_c}{\partial x_i \partial x_i} = \frac{\partial^2 \rho'}{\partial t^2} - \frac{\partial^2}{\partial x_i \partial x_j}(2\rho \tilde{u}_i u_j'' + \rho' \tilde{u}_i \tilde{u}_j) + 2\frac{\partial \tilde{u}_i}{\partial x_j}\frac{\partial \rho u_j''}{\partial x_i}. \tag{7.5d}$$

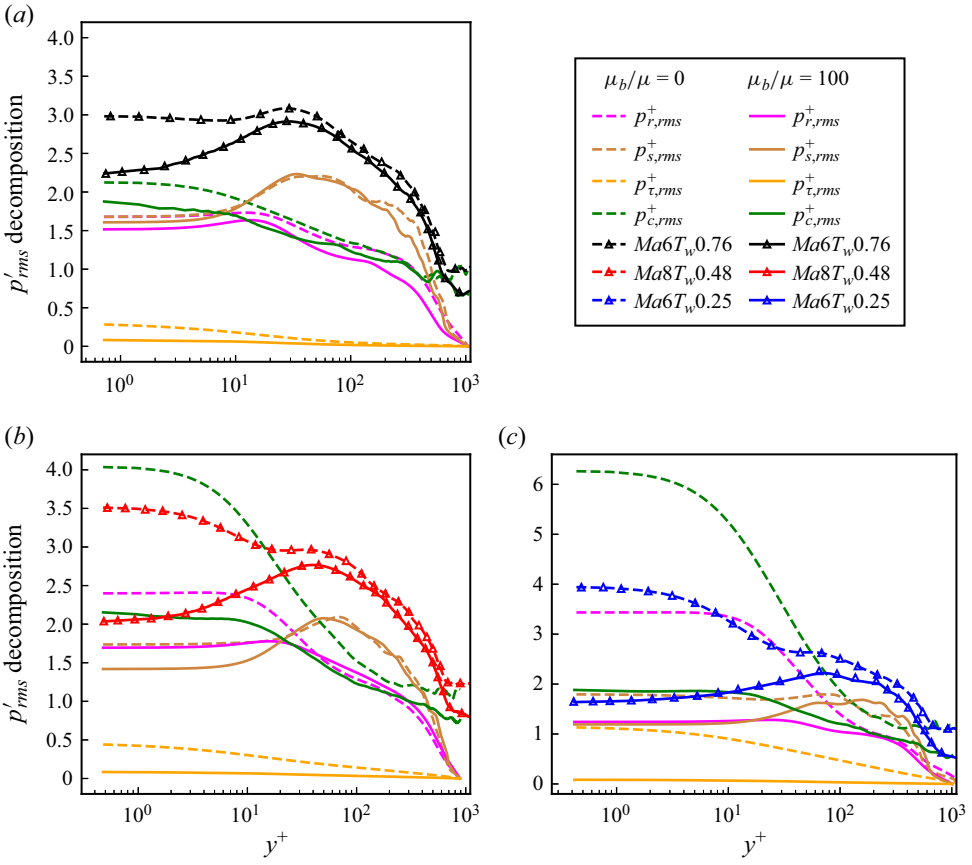

Figure 22. Wall-normal distributions of the r.m.s. pressure fluctuations p^+_{rms} and its components obtained from (7.5), which are normalized by τ_w in the inner scaling, for cases (*a*) $Ma6T_w0.76$, (*b*) $Ma8T_w0.48$ and (*c*) $Ma6T_w0.25$, with and without bulk viscosity. As shown in the legend, the dashed lines denote the cases without bulk viscosity ($\mu_b/\mu = 0$), while the solid lines denote the cases with bulk viscosity ($\mu_b/\mu = 100$). And the lines with symbols represent the pressure fluctuations p^+_{rms}, which is consistent with figure 9(*c*), while the lines without symbols represent its components.

These fluctuating pressure component equations are solved by performing second-order central difference in the streamwise and wall-normal directions, and by using the Fourier–Galerkin method in the spanwise direction, with boundary conditions and other details that can be found in Zhang *et al.* (2022).

To provide a quantitative explanation of the influence mechanism of bulk viscosity on fluctuating pressure, a comparative analysis of the r.m.s. pressure fluctuations p^+_{rms} and its components was conducted across different cases, as shown in figure 22. The reduction of both rapid pressure $p^+_{r,rms}$ and slow pressure $p^+_{s,rms}$ in the near-wall region is attributed to the influence of bulk viscosity, indicating that the bulk viscosity suppresses both linear mean shear–turbulence interactions and nonlinear turbulence–turbulence interactions, while the impact of bulk viscosity appears slightly more pronounced on the rapid pressure $p^+_{r,rms}$ than on the slow pressure $p^+_{s,rms}$. Due to its ability to mitigate the compressibility of the hypersonic turbulent boundary layer, bulk viscosity induces a substantial reduction in density fluctuations within the viscous sublayer and the buffer layer, consequently leading to a notable decrease in compressible pressure $p^+_{c,rms}$. With the Mach number

increase and the wall temperature decrease, the compressibility of the turbulent boundary layer is enhanced, and the influence of bulk viscosity is more significant. In addition, the viscous pressure $p^+_{\sigma,rms}$ also decreases due to the consideration of bulk viscosity. In the comprehensive analysis, while acknowledging the suppressive impact of bulk viscosity on incompressible pressure, it is essential to recognize that the compressible component of pressure fluctuations $p^+_{c,rms}$ experiences a pronounced reduction within the viscous sublayer and the buffer layer, which is attributed to the impact of bulk viscosity on the compressibility of the turbulent boundary layer.

8. Conclusion

In this paper, direct numerical simulations are performed for six cases with Mach numbers $Ma = 6, 8$, temperature ratios $T_w/T_r = 0.25, 0.48, 0.76$, and bulk-to-shear viscosity coefficient ratios $\mu_b/\mu = 0, 100$, respectively. We analyse comprehensively the effects of bulk viscosity on velocity-related variables, thermodynamic-related statistics, large-scale structures, and small-scale properties in the hypersonic compressible turbulent boundary layers.

The impact of bulk viscosity on mean statistics is found to be relatively small, with negligible effects on mean density and mean temperature. The transformed mean velocity profiles and Walz equation are minimally affected by bulk viscosity.

In contrast, the effect of bulk viscosity on fluctuating statistics is relatively significant. The wall-normal velocity fluctuation v''_{rms} is reduced significantly in the viscous sublayer by the enhanced viscous dissipation $-\bar{\rho}\epsilon_{yy}$ related to bulk viscosity in the wall-normal Reynolds stress budgets. The intensity of pressure fluctuations p'_{rms} in the near-wall region decreases distinctly after considering the bulk viscosity, which is attributed mainly to the reduction of compressible pressure fluctuations $p^+_{c,rms}$. The bulk viscosity leads to a slight decrease in the value of the turbulent Mach number, indicating that the bulk viscosity reduces the effect of the turbulence compressibility.

Regarding the turbulent kinetic energy budget, the pressure diffusion and pressure dilatation terms decrease significantly near the wall when considering bulk viscosity. The effect is attributed to the impact of bulk viscosity on decreasing fluid compressibility and density fluctuations near the wall.

The strong Reynolds analogy is mostly unaffected by bulk viscosity, with minimal influence on the correlation between temperature fluctuations and velocity fluctuations. The turbulent heat flux $\overline{\rho v'' T''}$ decreases slightly in the viscous sublayer by considering bulk viscosity. However, it exhibits little effect on the mean temperature and conductive heat flux $-k\,\partial T/\partial y$. As a consequence, the total heat flux in the viscous sublayer is decreased by bulk viscosity.

When considering bulk viscosity, the large-scale vortex structure based on the Q-criterion becomes fragmented in the outer layer of the turbulent boundary layer, while the small-scale vortex structure becomes richer. Additionally, the intensity of the travelling-wave-like alternating positive and negative structures of instantaneous pressure field $p'/\bar{p}$ in the near-wall region decreases distinctly.

In terms of small-scale properties, bulk viscosity gives a significant impact on the near-wall region of the turbulent boundary layer. The intensity of turbulent fluctuations and shear effects in the viscous sublayer is stronger compared to compressible homogeneous isotropic turbulence and homogeneous shear turbulence. Furthermore, the bulk viscosity decreases the fluctuating velocity derivative with respect to the streamwise coordinate $\partial u'/\partial x$ within the viscous sublayer, and the probability density function (PDF) for the

absolute value of the fluctuating velocity derivative $|\partial u'/\partial x|$ greater than 5 decreases. However, the effect of bulk viscosity on the fluctuating velocity derivative with respect to the wall-normal coordinate $\partial u'/\partial y$ is negligible. Moreover, the PDF of the velocity divergence $\theta = \partial u_i/\partial x_i$ decreases in the turbulent boundary layer, indicating weakened fluid compressibility when considering bulk viscosity.

The compressibility of the hypersonic turbulent boundary layer is weakened in the near-wall region by considering bulk viscosity, which is manifested most clearly by a reduction of the pressure fluctuations p'_{rms} by approximately 25 % in the viscous sublayer. And this effect becomes more significant as the Mach number increases and the wall temperature decreases. By analysing comprehensively the existing results, this paper concludes that when the bulk-to-shear viscosity ratio of the gas reaches a few hundred levels ($\mu_b/\mu = O(10^2)$), and the mechanical behaviour of the near-wall region ($y^+ \leq 30$) of the turbulent boundary layer is of greater interest, the impact of bulk viscosity on the hypersonic cold-wall turbulent boundary layer may not be negligible.

Acknowledgements. The authors gratefully acknowledge the Institute of Extreme Mechanics of Northwestern Polytechnical University and computing resources provided by Hefei Advanced Computing Center. And the authors are particularly grateful to Dr Peng-jun-yi Zhang from the University of Science and Technology of China, who provided us with the code for the fluctuating pressure decomposition.

Funding. This research is supported by the National Natural Science Foundation of China (nos 12388101, 92371103 and 11972272).

Declaration of interests. The authors report no conflict of interest.

Data availability statement. Data available on request from the authors.

Author ORCIDs.
Chaoyu Zheng https://orcid.org/0009-0009-1538-4311;
Yongliang Feng https://orcid.org/0000-0002-2707-6529;
Xiaojing Zheng https://orcid.org/0000-0002-6845-2949.

References

Bernardini, M. & Pirozzoli, S. 2011 Inner/outer layer interactions in turbulent boundary layers: a refined measure for the large-scale amplitude modulation mechanism. *Phys. Fluids* **23** (6), 061701.

Boukharfane, R., Ferrer, P.J.M., Mura, A. & Giovangigli, V. 2019 On the role of bulk viscosity in compressible reactive shear layer developments. *Eur. J. Mech.* – B/*Fluids* **77**, 32–47.

Bross, M., Scharnowski, S. & Khler, C.J. 2021 Large-scale coherent structures in compressible turbulent boundary layers. *J. Fluid Mech.* **911**, A2.

Bruno, D. & Giovangigli, V. 2022 Internal energy relaxation processes and bulk viscosities in fluids. *Fluids* **7** (11), 356.

Chen, S., Wang, X., Wang, J., Wan, M. & Chen, S. 2019 Effects of bulk viscosity on compressible homogeneous turbulence. *Phys. Fluids* **31** (8), 085115.

Cheng, C., Chen, X., Zhu, W., Shyy, W. & Fu, L. 2024 Progress in physical modeling of compressible wall-bounded turbulent flows. *Acta Mechanica Sin.* **40**, 323663.

Cogo, M., Salvadore, F., Picano, F. & Bernardini, M. 2022 Direct numerical simulation of supersonic and hypersonic turbulent boundary layers at moderate-high Reynolds numbers and isothermal wall condition. *J. Fluid Mech.* **945**, A30.

Coleman, G.N., Kim, J. & Moser, R.D. 1995 A numerical study of turbulent supersonic isothermal-wall channel flow. *J. Fluid Mech.* **305**, 159–183.

Cramer, M.S. 2012 Numerical estimates for the bulk viscosity of ideal gases. *Phys. Fluids* **24** (6), 531.

Cramer, M.S. & Bahmani, F. 2014 Effect of large bulk viscosity on large-Reynolds-number flows. *J. Fluid Mech.* **751**, 142–163.

DeGottardi, W. & Matveev, K.A. 2023 Viscous dissipation in a gas of one-dimensional fermions with generic dispersion. *Phys. Rev.* B **107**, 075442.

DONG, S., TONG, F., YU, M., CHEN, J., YUAN, X. & WANG, Q. 2022 Positive and negative pairs of fluctuating wall shear stress and heat flux in supersonic turbulent boundary layers. *Phys. Fluids* **34** (8), 085115.

VAN DREIST, E.R. 1956 The problem of aerodynamic heating. *Aeronaut. Engng Rev.* **15** (10), 26–41.

DUAN, L., BEEKMAN, I. & MARTÍN, M.P. 2010 Direct numerical simulation of hypersonic turbulent boundary layers. Part 2. Effect of wall temperature. *J. Fluid Mech.* **655**, 419–445.

DUAN, L., BEEKMAN, I. & MARTÍN, M.P. 2011 Direct numerical simulation of hypersonic turbulent boundary layers. Part 3. Effect of Mach number. *J. Fluid Mech.* **672**, 245–267.

DUAN, L., CHOUDHARI, M.M. & ZHANG, C. 2016 Pressure fluctuations induced by a hypersonic turbulent boundary layer. *J. Fluid Mech.* **804**, 578–607.

DUAN, L. & MARTÍN, M.P. 2011 Direct numerical simulation of hypersonic turbulent boundary layers. Part 4. Effect of high enthalpy. *J. Fluid Mech.* **684**, 25–59.

EMANUEL, G. 1992 Effect of bulk viscosity on a hypersonic boundary layer. *Phys. Fluids* A*: Fluid Dyn.* **4** (3), 491–495.

EU, B.C. & OHR, Y.G. 2001 Generalized hydrodynamics, bulk viscosity, and sound wave absorption and dispersion in dilute rigid molecular gases. *Phys. Fluids* **13** (3), 744–753.

FU, L., KARP, M., BOSE, S.T., MOIN, P. & URZAY, J. 2021 Shock-induced heating and transition to turbulence in a hypersonic boundary layer. *J. Fluid Mech.* **909**, A8.

GAVIGLIO, J. 1987 Reynolds analogies and experimental study of heat transfer in the supersonic boundary layer. *Intl J. Heat Mass Transfer* **30** (5), 911–926.

GRAVES, R.E. & ARGROW, B.M. 1999 Bulk viscosity: past to present. *J. Thermophys. Heat Transfer* **13** (3), 337–342.

GRIFFIN, K.P., FU, L. & MOIN, P. 2021 Velocity transformation for compressible wall-bounded turbulent flows with and without heat transfer. *Proc. Natl Acad. Sci.* **118** (34), e2111144118.

GU, Z. & UBACHS, W. 2014 A systematic study of Rayleigh–Brillouin scattering in air, N_2, and O_2 gases. *J. Chem. Phys.* **141** (10), 104320.

GUARINI, S., MOSER, R., SHARIFF, K. & WRAY, A. 2000 Direct numerical simulation of a supersonic turbulent boundary layer at Mach 2.5. *J. Fluid Mech.* **414**, 1–33.

HOU, Y., JIN, K., FENG, Y. & ZHENG, X. 2023 High-order targeted essentially non-oscillatory scheme for two-fluid plasma model. *Appl. Math. Mech.* **44** (6), 941–960.

HUANG, J., DUAN, L. & CHOUDHARI, M.M. 2022 Direct numerical simulation of hypersonic turbulent boundary layers: effect of spatial evolution and Reynolds number. *J. Fluid Mech.* **937**, A3.

HUANG, J., NICHOLSON, G.L., DUAN, L., CHOUDHARI, M.M. & BOWERSOX, R.D. 2020 Simulation and modeling of cold-wall hypersonic turbulent boundary layers on flat plate. In *AIAA Scitech 2020 Forum*.

HUANG, P.G., COLEMAN, G.N. & BRADSHAW, P. 1995 Compressible turbulent channel flows: DNS results and modelling. *J. Fluid Mech.* **305**, 185–218.

HUNT, J.C.R., WRAY, A.A. & MOIN, P. 1988 Eddies, streams, and convergence zones in turbulent flows. Center for Turbulence Research.

JAEGER, F., MATAR, O.K. & MÜLLER, E.A. 2018 Bulk viscosity of molecular fluids. *J. Chem. Phys.* **148** (17), 174504.

JIANG, G.-S. & SHU, C.-W. 1996 Efficient implementation of weighted ENO schemes. *J. Comput. Phys.* **126** (1), 202–228.

JIMÉNEZ, J. 2013 Near-wall turbulence. *Phys. Fluids* **25** (10), 101302.

KOSUGE, S. & AOKI, K. 2022 Navier–Stokes equations and bulk viscosity for a polyatomic gas with temperature-dependent specific heats. *Fluids* **8** (1), 5.

KUSTOVA, E., MEKHONOSHINA, M. & KOSAREVA, A. 2019 Relaxation processes in carbon dioxide. *Phys. Fluids* **31** (4), 046104.

LAGHA, M., KIM, J., ELDREDGE, J.D. & ZHONG, X. 2011 A numerical study of compressible turbulent boundary layers. *Phys. Fluids* **23** (1), 187.

LEE, H., HELM, C., MARTÍN, P.M. & WILLIAMS, O.J.H. 2023 Compressible boundary layer velocity transformation based on a generalized form of the total stress. *Phys. Rev. Fluids* **8**, 074604.

LELE, S.K. 1994 Compressibility effects on turbulence. *Annu. Rev. Fluid Mech.* **26** (1), 211–254.

LI, J.Y., YU, M., SUN, D., LIU, P.X. & YUAN, X.X. 2022 Wall heat transfer in high-enthalpy hypersonic turbulent boundary layers. *Phys. Fluids* **34** (8), 085102.

LI, Q. & WU, L. 2022 A kinetic model for rarefied flows of molecular gas with vibrational modes. arXiv:2201.06855

LI, X.L., FU, D.X. & MA, Y.W. 2006 Direct numerical simulation of a spatially evolving supersonic turbulent boundary layer at $Ma = 6$. *Chinese Phys. Lett.* **23** (6), 1519.

LIAO, W., PENG, Y. & LUO, L.-S. 2009 Gas-kinetic schemes for direct numerical simulations of compressible homogeneous turbulence. *Phys. Rev.* E **80**, 046702.

LIU, Q., LUO, Z., TU, G., DENG, X., CHENG, P. & ZHANG, P. 2021 Direct numerical simulations of a supersonic turbulent boundary layer subject to velocity–temperature coupled control. *Phys. Rev. Fluids* **6**, 044603.

MANSOUR, N.N., KIM, J. & MOIN, P. 1988 Reynolds-stress and dissipation-rate budgets in a turbulent channel flow. *J. Fluid Mech.* **194**, 15–44.

MARTIN, M.P. 2007 Direct numerical simulation of hypersonic turbulent boundary layers. Part 1. Initialization and comparison with experiments. *J. Fluid Mech.* **570**, 347–364.

MO, F., LI, Q., ZHANG, L. & GAO, Z. 2023 Direct numerical simulation of hypersonic wall-bounded turbulent flows: an improved inflow boundary condition and applications. *Phys. Fluids* **35** (3), 035135.

MORKOVIN, M.V. 1962 Effects of compressibility on turbulent flows. *Méc. Turbul.* **367** (380), 26.

NICHOLSON, G.L., HUANG, J., DUAN, L., CHOUDHARI, M.M., MORREALE, B. & BOWERSOX, R.D. 2022 Budgets of Reynolds stresses and turbulent heat flux for hypersonic turbulent boundary layers subject to pressure gradients. In *AIAA SCITECH 2022 Forum*, p. 1059.

OU, J., WANG, C. & CHEN, J. 2024 Rarefaction effects on hypersonic boundary-layer stability. *Acta Mechanica Sin.* **40** (3), 123184.

PAN, S. & JOHNSEN, E. 2017 The role of bulk viscosity on the decay of compressible, homogeneous, isotropic turbulence. *J. Fluid Mech.* **833**, 717–744.

PAN, X., SHNEIDER, M.N. & MILES, R.B. 2004 Coherent Rayleigh–Brillouin scattering in molecular gases. *Phys. Rev.* A **69** (3), 033814.

PAN, X., SHNEIDER, M.N. & MILES, R.B. 2005 Power spectrum of coherent Rayleigh–Brillouin scattering in carbon dioxide. *Phys. Rev.* A **71** (4), 45801.

PASSIATORE, D., SCIACOVELLI, L., CINNELLA, P. & PASCAZIO, G. 2021 Direct numerical simulation of a hypersonic boundary layer in chemical non-equilibrium. In *55th 3AF International Conference on Applied Aerodynamics*.

PASSIATORE, D., SCIACOVELLI, L., CINNELLA, P. & PASCAZIO, G. 2022 Thermochemical non-equilibrium effects in turbulent hypersonic boundary layers. *J. Fluid Mech.* **941**, A21.

PIROZZOLI, S., GRASSO, F. & GATSKI, T.B. 2004 Direct numerical simulation and analysis of a spatially evolving supersonic turbulent boundary layer at $M = 2.25$. *Phys. Fluids* **16** (3), 530–545.

PIROZZOLI, S., ROMERO, J., FATICA, M., VERZICCO, R. & ORLANDI, P. 2021 One-point statistics for turbulent pipe flow up to $Re_\tau \approx 6000$. *J. Fluid Mech.* **926**, A28.

PRANGSMA, G.J., ALBERGA, A.H. & BEENAKKER, J.J.M. 1973 Ultrasonic determination of the volume viscosity of N_2, CO, CH_4 and CD_4 between 77 and 300 K. *Physica* **64** (2), 278–288.

RENZO, M.D. & URZAY, J. 2021 Direct numerical simulation of a hypersonic transitional boundary layer at suborbital enthalpies. *J. Fluid Mech.* **912**, A29.

RUBESIN, M.W. 1990 Extra compressibility terms for Favre-averaged two-equation models of inhomogeneous turbulent flows. *Tech. Rep.*

SARKAR, S., ERLEBACHER, G., HUSSAINI, M.Y. & KREISS, H.O. 1991 The analysis and modelling of dilatational terms in compressible turbulence. *J. Fluid Mech.* **227**, 473–493.

SHARMA, B. & KUMAR, R. 2023 A brief introduction to bulk viscosity of fluids. arXiv:2303.08400

SHARMA, B., PAREEK, S. & KUMAR, R. 2023 Bulk viscosity of dilute monatomic gases revisited. *Eur. J. Mech. – B/Fluids* **98**, 32–39.

SMITS, A.J., HULTMARK, M., LEE, M., PIROZZOLI, S. & WU, X. 2021 Reynolds stress scaling in the near-wall region of wall-bounded flows. *J. Fluid Mech.* **926**, A31.

STOKES, G.G. 1851 On the effect of the internal friction of fluids on the motion of pendulums. *Trans. Camb. Phil. Soc.* **9**, 8–106.

TANG, J., ZHAO, Z., WAN, Z.-H. & LIU, N.-S. 2020 On the near-wall structures and statistics of fluctuating pressure in compressible turbulent channel flows. *Phys. Fluids* **32** (11), 115121.

TISZA, L. 1942 Supersonic absorption and Stokes' viscosity relation. *Phys. Rev.* **61** (7–8), 531.

TOUBER, E. 2019 Small-scale two-dimensional turbulence shaped by bulk viscosity. *J. Fluid Mech.* **875**, 974–1003.

TRETTEL, A. & LARSSON, J. 2016 Mean velocity scaling for compressible wall turbulence with heat transfer. *Phys. Fluids* **28** (2), 026102.

VIEITEZ, M.O., VAN DUIJN, E.-J., UBACHS, W., WITSCHAS, B., MEIJER, A., DE WIJN, A.S., DAM, N.J. & VAN DE WATER, W. 2010 Coherent and spontaneous Rayleigh–Brillouin scattering in atomic and molecular gases and gas mixtures. *Phys. Rev.* A **82** (4), 043836.

VINCENTI, W.G. & KRUGER, C.H. 1965 *Introduction to Physical Gas Dynamics*. Wiley.

VOLPIANI, P.S., IYER, P.S., PIROZZOLI, S. & LARSSON, J. 2020 Data-driven compressibility transformation for turbulent wall layers. *Phys. Rev. Fluids* **5**, 052602.

WALZ, A. 1969 *Boundary Layers of Flow and Temperature*. MIT Press.

XU, D., WANG, J. & CHEN, S. 2022 Skin-friction and heat-transfer decompositions in hypersonic transitional and turbulent boundary layers. *J. Fluid Mech.* **941**, A4.

XU, D., WANG, J. & CHEN, S. 2023 Reynolds number and wall cooling effects on correlations between the thermodynamic variables in hypersonic turbulent boundary layers. *J. Fluid Mech.* **965**, A4.

XU, D., WANG, J., WAN, M., YU, C. & CHEN, S. 2021*a* Compressibility effect in hypersonic boundary layer with isothermal wall condition. *Phys. Rev. Fluids* **6** (5), 054609.

XU, D., WANG, J., WAN, M., YU, C., LI, X. & CHEN, S. 2021*b* Effect of wall temperature on the kinetic energy transfer in a hypersonic turbulent boundary layer. *J. Fluid Mech.* **929**, A33.

YU, M., XU, C.-X. & PIROZZOLI, S. 2020 Compressibility effects on pressure fluctuation in compressible turbulent channel flows. *Phys. Rev. Fluids* **5** (11), 113401.

ZHANG, C., DUAN, L. & CHOUDHARI, M.M. 2017 Effect of wall cooling on boundary-layer-induced pressure fluctuations at Mach 6. *J. Fluid Mech.* **822**, 5–30.

ZHANG, C., DUAN, L. & CHOUDHARI, M.M. 2018 Direct numerical simulation database for supersonic and hypersonic turbulent boundary layers. *AIAA J.* **56** (11), 4297–4311.

ZHANG, P.-J.-Y., WAN, Z.-H., LIU, N.-S., SUN, D.-J. & LU, X.-Y. 2022 Wall-cooling effects on pressure fluctuations in compressible turbulent boundary layers from subsonic to hypersonic regimes. *J. Fluid Mech.* **946**, A14.

ZHANG, Y.-S., BI, W.-T., HUSSAIN, F. & SHE, Z.-S. 2014 A generalized Reynolds analogy for compressible wall-bounded turbulent flows. *J. Fluid Mech.* **739**, 392–420.

ZHU, Y., ZHANG, C., CHEN, X., YUAN, H., WU, J., CHEN, S., LEE, C. & GAD-EL HAK, M. 2016 Transition in hypersonic boundary layers: role of dilatational waves. *AIAA J.* **54** (10), 3039–3049.

ZUCKERWAR, A.J. & ASH, R.L. 2006 Variational approach to the volume viscosity of fluids. *Phys. Fluids* **18** (4), 047101.